Condensation of pericentrin proteins in human cells illuminates phase separation in centrosome assembly

Xueer Jiang[1], Dac Bang Tam Ho[1], Karan Mahe[1], Jennielee Mia[1], Guadalupe Sepulveda[1†], Mark Antkowiak[1‖], Soichiro Yamada[2], and Li-En Jao[1*]

Affiliations

[1]Department of Cell Biology and Human Anatomy, University of California, Davis, School of Medicine, Davis, CA 95616, USA

[2]Department of Biomedical Engineering, University of California, Davis, Davis, CA 95616, USA

[†]Current address: Department of Molecular and Cell Biology, University of California, Berkeley, Berkeley, CA 94720, USA

[‖]Current address: Northwestern University, Feinberg School of Medicine, Chicago, IL 60611, USA

[*]For correspondence: ljao@ucdavis.edu

Abstract

Mitotic centrosomes are complex membraneless organelles that guide the formation of mitotic spindles to ensure faithful cell division. They are formed by timely expansion of the pericentriolar material (PCM) around the centrioles at the onset of mitosis. How PCM proteins are recruited and held together without a lipid membrane remains elusive. Here we found that endogenously expressed pericentrin (PCNT), a conserved PCM scaffold protein, condenses into liquid-like granules during early mitosis in cultured human cells. Furthermore, the N-terminal segment of PCNT, enriched with conserved coiled-coils and low-complexity regions (LCRs), undergoes phase separation. These PCNT “condensates” selectively recruit PCM components and nucleate microtubules in cells. We propose that coiled-coils and LCRs, two prevalent sequence features in the centrosomal proteome, are preserved under evolutionary pressure to drive phase separation, a process that bestows upon the centrosome a distinct material property critical for its assembly and functions.

Introduction

The centrosome serves as a major microtubule-organizing center (MTOC) in animal cells. It consists of a pair of centrioles embedded in a proteinaceous network of pericentriolar material (PCM) (Conduit et al., 2015; Rieder & Borisy, 1982; Vorobjev & Chentsov Yu, 1982; Wang et al., 2011; Woodruff et al., 2014). The MTOC activity of the centrosome is determined by the PCM, which acts as a scaffold to recruit MT regulators and nucleators, such as γ-tubulin ring complexes (γ-TuRCs) (Jeng & Stearns, 1999; Moritz, Braunfeld, Sedat, et al., 1995; Moritz et al., 1998; Oegema et al., 1999; Zheng et al., 1995). The PCM is not a static structure. In interphase cells, relatively small amounts of PCM are assembled around the centriole and organized as a layered, nanometer-sized toroid (Fu & Glover, 2012; Lawo et al., 2012; Mennella et al., 2012; Sonnen et al., 2012). As the cell enters mitosis, the PCM expands dramatically into a micron-sized ensemble, with a concomitant increase in its MTOC activity as the mitotic spindle forms in a process termed centrosome maturation (Mahen & Venkitaraman, 2012; Mennella et al., 2014; Palazzo et al., 2000).

Over the past decades, proteins important for centrosome maturation have been identified (Andersen et al., 2003; Dobbelaere et al., 2008; Goshima et al., 2007; Hamill et al., 2002; Hutchins et al., 2010; Neumann et al., 2010; Sonnichsen et al., 2005; Woodruff et al., 2015). At the molecular level, centrosome maturation is initiated upon phosphorylation of core PCM components, such as spindle-defective protein 5 (SPD-5), centrosomin (Cnn), and pericentrin (PCNT) by mitotic kinases Polo/PLK1 and aurora kinase A (Barr & Gergely, 2007; Berdnik & Knoblich, 2002; Conduit, Feng, et al., 2014; Hannak et al., 2001; Joukov et al., 2014; Kinoshita et al., 2005; Lee & Rhee, 2011; Woodruff et al., 2017; Woodruff et al., 2015; Wueseke et al., 2016). This triggers the cooperative assembly of additional PCM proteins (Alvarez-Rodrigo et al., 2019; Conduit, Richens, et al., 2014; Hamill et al., 2002; Kemp et al., 2004; Meng et al.,

57 2015) and γ-TuRCs to facilitate bipolar spindle assembly (Conduit et al., 2015; Jeng & Stearns,
58 1999; Khodjakov & Rieder, 1999; Moritz, Braunfeld, Sedat, et al., 1995; Moritz et al., 1998;
59 Oegema et al., 1999; Piehl et al., 2004; Woodruff et al., 2014; Zheng et al., 1995). While the
60 mechanism of centrosome maturation has been elucidated at the molecular level, the
61 biophysical principle of PCM assembly remains elusive at the organellar level—without an
62 enclosing membrane, what keeps the crowded PCM proteins from dispersing?

63 Liquid-liquid phase separation, a process through which macromolecules de-mix and
64 partition from a single phase into two or more distinct phases in a concentration-dependent
65 manner, has emerged as a mechanism that underlies a variety of cellular processes involving
66 non-membrane-bound compartments or organelles (reviews in Banani et al., 2017; Holehouse &
67 Pappu, 2018; Hyman et al., 2014; Shin & Brangwynne, 2017). Recently Woodruff and
68 colleagues proposed that the centrosome is formed through phase separation (Woodruff et al.,
69 2017). They showed that *in vitro* purified SPD-5, a core PCM protein with extensive coiled-coils
70 in *C. elegans* (Hamill et al., 2002), forms spherical liquid "condensates" *in vitro* in the presence
71 of crowding reagents, which mimic the dense cytoplasm (Woodruff et al., 2017). SPD-5
72 condensates possess a centrosomal activity *in vitro*, capable of nucleating MTs after selectively
73 recruiting tubulin dimers and cognate proteins (ZYG-9 and TPXL-1) (Woodruff et al., 2017).
74 These data are also consistent with mathematical modeling of centrosomes as autocatalytic
75 droplets formed by phase separation (Zwicker et al., 2014). However, it is unclear how closely
76 this *in vitro* system actually reflects centrosomal MT nucleation *in vivo*, as SPD-5 condensates
77 do not recruit γ-tubulin, an essential *in vivo* MT nucleation factor for many species (Felix et al.,
78 1994; Hannak et al., 2002; Joshi et al., 1992; Oakley et al., 1990; Stearns et al., 1991; Stearns
79 & Kirschner, 1994; Zheng et al., 1991).

80 Contrary data suggest that phase separation may not play a role in centrosome assembly.
81 For example, Cnn—a major mitotic PCM component and functional homolog of SPD-5 in

82 *Drosophila*—does not undergo dynamic internal rearrangements as it incorporates into the
83 centrosome *in vivo* (Conduit et al., 2010; Conduit, Feng, et al., 2014). Two short conserved
84 domains of Cnn can self-assemble into solid-like scaffolds *in vitro*, but no liquid-to-solid phase
85 transition has been observed (Feng et al., 2017). However, the action of these Cnn segments in
86 the context of full-length Cnn *in vivo* remains unknown. Together, with the available evidence, it
87 remains elusive whether liquid-liquid phase separation underlies centrosome assembly.
88 In vertebrates, PCNT plays a particularly important role in PCM assembly as it is required for
89 the initiation (Lee & Rhee, 2011; Zimmerman et al., 2004) and recruitment of key PCM
90 components during centrosome maturation (Haren et al., 2009; Lawo et al., 2012; Zimmerman
91 et al., 2004). We recently showed that PCNT enrichment during centrosome maturation is
92 controlled by a co-translational targeting mechanism that ensures timely production and spatial
93 deposition of PCNT at the centrosome (Sepulveda et al., 2018). Indeed, PCNT expression is
94 tightly regulated. For example, human loss-of-function mutations of PCNT cause microcephalic
95 osteodysplastic primordial dwarfism type II (Anitha et al., 2009; Delaval & Doxsey, 2010; Griffith
96 et al., 2008; Numata et al., 2009; Rauch et al., 2008), whereas elevated PCNT levels disrupt
97 ciliary protein trafficking and sonic hedgehog signaling, and may contribute to clinical features of
98 Down syndrome (Galati et al., 2018). Despite its importance at the cellular and organismal
99 levels, the precise function of PCNT in centrosome assembly remains enigmatic.
100 Here we demonstrate that endogenously GFP-tagged human PCNT forms droplet-like
101 pericentrosomal granules during early mitosis. These GFP-PCNT granules show liquid-like
102 properties as they fuse and split in seconds and are dissolved by hexanediol that disrupts weak
103 protein-protein interactions. These data suggest that PCNT phase separates into liquid-like
104 condensates at physiologically relevant levels during mitosis. We further show that phase
105 separation of PCNT is driven by the segments enriched with conserved coiled-coils and low-
106 complexity regions (LCRs). These PCNT condensates transition from liquid- to gel/solid-like

107 states and exhibit centrosome-like activities in cells, including selectively recruiting endogenous
108 PCM components and nucleating MTs. The finding that PCNT undergoes liquid-liquid phase
109 separation under physiologically relevant conditions provides insights into the role of coiled-coils
110 and LCRs in the assembly of the membraneless centrosome, which is enriched with proteins
111 containing both sequence features.

112 **Results**

113 **Endogenously expressed GFP-PCNT forms liquid-like condensates during early mitosis**

114 To test whether PCNT undergoes liquid-liquid phase separation under physiologically
115 relevant conditions in mammalian cells, we generated stable human cell lines with GFP-tagged
116 PCNT expressed from its endogenous locus using the CRISPR technology (S. Lin et al., 2014;
117 Zhang et al., 2017). We inserted a super-folder GFP (sfGFP) cassette at the 5' end (exon 1) of
118 the *PCNT* allele in hTERT-immortalized human retinal pigment epithelial cells (RPE-1 cells)
119 (**Figure 1- figure supplement 1**). The resulting knock-in cell lines exhibited normal cell
120 morphology and mitotic progression with the GFP-PCNT decorating the centrosomes as
121 expected (**Figure 1- figure supplement 1**).

122 Through high-resolution time-lapse confocal microscopy, we observed small GFP-PCNT
123 granules (100-400 nm) near centrosomes in early mitosis (**Figure 1A and Figure 1- movie**
124 **supplement 1 and 2**). Similar pericentrosomal PCNT granules were also observed by
125 immunostaining endogenous, untagged PCNT during early mitosis (Sepulveda et al., 2018)
126 (**Figure 1- figure supplement 2**). These GFP-PCNT granules were dynamic and appeared to
127 fuse and split over a timescale of seconds. Similar dynamic pericentrosomal GFP-PCNT
128 granules were also observed in another independent knock-in clone (**Figure 1- movie**
129 **supplement 3**). This dynamic behavior suggests that these PCNT granules may be liquid-like
130 condensates formed by liquid-liquid phase separation. To test this hypothesis, we treated the
131 cells with aliphatic alcohol 1,6-hexanediol, which dissolves liquid-like condensates by disrupting
132 weak hydrophobic interactions (Kroschwald et al., 2017; Ribbeck & Gorlich, 2002). Following
133 hexanediol addition, PCNT granules near centrosomes dispersed within minutes (**Figure 1B**
134 **and C**). Together, these results suggest that PCNT, expressed from its endogenous locus,

135 forms liquid-like condensates, likely through liquid-liquid phase separation, before incorporating
136 into the early mitotic centrosome of cultured human cells.
137

138 **Coiled-coils and low-complexity regions of pericentrin are more conserved than the rest**
139 **of the protein sequence**

140 If condensation of PCNT is of evolutionary significance, the sequence features that
141 contribute to condensation should be conserved across species and may be identifiable at the
142 primary sequence level. To test this hypothesis, we constructed an alignment of 169 pericentrin
143 orthologous proteins—167 from vertebrates, one from fruit fly (D-PLP, Martinez-Campos et al.,
144 2004), and one from budding yeast (Spc110, Knop & Schiebel, 1997; Sundberg & Davis, 1997)
145 (**Figure 2A and Figure 2- table 1**). A number of sequence blocks are highly conserved. A
146 prominent one is located at the C-terminus, particularly at the PACT motif, a hallmark pericentrin
147 domain known for centrosomal anchoring (Gillingham & Munro, 2000; Takahashi et al., 2002).
148 Another highly conserved region is in the middle portion of the protein. In contrast, the N-
149 terminus is not well conserved, with the evidence of clade-specific insertions.

150 To gain insights into the properties of these conserved sequences, we performed further *in*
151 *silico* analyses (Lupas et al., 1991; Wootton, 1994), focusing on human PCNT. We found that
152 similar to other centrosomal proteins, human PCNT is enriched with coiled-coils and low-
153 complexity regions (LCRs) (**Figure 2A**). LCRs often overlap with intrinsically disordered regions,
154 which can mediate multivalent interactions to drive or tune liquid-liquid phase separation (Boke
155 et al., 2016; Kato et al., 2012; Lin et al., 2015; Molliex et al., 2015; Patel et al., 2015; Riback et
156 al., 2017). Indeed some disorder predictors (e.g., PONDR, Peng et al., 2006; Peng et al., 2005)
157 predicted that human PCNT is largely disordered except for the C-terminal PACT motif (**Figure**
158 **2- figure supplement 1**). However, as a known limitation with current disorder predictions

159 (Atkins et al., 2015), not all disorder predictors are in complete agreement, with each predictor
160 suggesting different degrees of disorder/order tendency [e.g., IUpred (Dosztanyi et al., 2005)
161 predicted an overall more ordered structure than PONDR did].
162 Nonetheless, by comparing the conservation profile of the multi-species alignment and the
163 locations of the predicted features of human PCNT, we found that the coiled-coils and LCRs in
164 human PCNT are concentrated within the conserved orthologous regions (**Figure 2A**).
165 Statistical analyses further demonstrated that coiled-coils and LCRs are significantly more
166 conserved than non-coiled-coils and non-LCRs, respectively, in human PCNT (**Figure 2B**).
167 Together, these results suggest that coiled-coils and LCRs of pericentrin orthologs are likely
168 under natural selection to preserve their molecular functions.
169

170 **PCNT phase separates via its coiled-coil/LCR-rich segments in a concentration-**
171 **dependent manner**

172 Given that both coiled-coils and LCRs can drive liquid-liquid phase separation (Berry et al.,
173 2015; Boeynaems et al., 2018; Elbaum-Garfinkle et al., 2015; Fang et al., 2019; Hennig et al.,
174 2015; Lu et al., 2020; Molliex et al., 2015; Nott et al., 2015; Smith et al., 2016; Wang et al.,
175 2018; Wippich et al., 2013; Zeng et al., 2016; Zhang et al., 2018), we hypothesized that the
176 coiled-coil/LCR-rich sequences drive phase separation of the full-length PCNT observed in the
177 knock-in cells.
178 To test this hypothesis, control PCNT transcription tightly, and map phase separation
179 determinants, we divided PCNT into N- and C-terminal segments, tagged each with sfGFP, and
180 subcloned the resulting GFP-PCNT constructs under the control of a doxycycline (Dox)-
181 inducible promoter. We then stably integrated each construct in RPE-1 cells using a *piggyBac*
182 transposon system (Kim et al., 2016). Upon Dox induction, live cell imaging showed that the N-

183 terminal segment, GFP-PCNT (2-1960), formed dynamic condensates (**Figure 2C and Figure**
184 **2- movie supplement 1**) with fast internal rearrangement of molecules ($t_{1/2}$ = 260 ms) as
185 determined by fluorescence recovery after photobleaching (FRAP) assays (**Figure 2D**). In
186 contrast, the C-terminal segment, GFP-PCNT (1954-3336), formed solid-like scaffolds (**Figure**
187 **2C and Figure 2- movie supplement 2**) with little internal rearrangement or fluorescence
188 recovery (**Figure 2D**).

189 To further map the phase separation driver sequences, we tested GFP-tagged PCNT (2-
190 891) and (854-1960) constructs, which subdivide PCNT (2-1960) but do not disrupt predicted
191 individual coiled-coils or LCRs. After inducing their expression in cells, we compared their
192 respective critical concentrations, the point above which liquid-liquid phase separation occurs
193 (Asherie, 2004). To quantitatively assess this value in living cells, we developed an imaging and
194 quantification workflow to measure relative protein concentrations by fluorescence intensity per
195 voxel (volume). With this workflow, we found that GFP-PCNT (2-891) remained diffuse in cells
196 as its concentration increased. However, over the same concentration range, GFP-PCNT (854-
197 1960) suddenly formed droplet-like condensates when it reached its critical concentration for
198 phase separation (**Figure 2E,** also see **Figure 3**). Using this workflow, we also validated the
199 liquid-liquid phase separation behavior of GFP-PCNT (2-1960)—which had a slightly higher
200 critical concentration than GFP-PCNT (854-1960)—and the lack of phase separation for GFP-
201 PCNT (1954-3336) within the same concentration range (**Figure 2E**). Collectively, these results
202 suggest that the abundant coiled-coils and LCRs between residues 854 and 1960 of human
203 PCNT—which are also well conserved across species (**Figure 2A and B**)—contain the key
204 sequence elements that mediate PCNT phase separation.

205 **GFP-PCNT (854-1960) undergoes liquid-liquid phase separation, coalesces, and moves**
206 **toward the centrosome**

207 Besides phase separating at a lower concentration than GFP-PCNT (2-1960) (**Figure 2E**),
208 GFP-PCNT (854-1960) condensates also exhibited different morphology and behavior. In
209 particular, early-stage small GFP-PCNT (854-1960) condensates formed well-defined spherical,
210 liquid-like droplets as they rapidly split and fused within seconds (**Figure 3A**). Over time, these
211 GFP-PCNT (854-1960) condensates coalesced and converged at the centrosome—arcing
212 around the nucleus in some cases—to form large pericentrosomal blobs (**Figure 3B and Figure**
213 **3- movie supplement 1**). Their movement is likely mediated by dynein motors as this PCNT
214 segment contains a putative dynein-binding domain (Tynan et al., 2000) (**Figure 2A**).
215 Importantly, since FLAG- and mScarlet-i-tagged PCNT (854-1960) fusion proteins also formed
216 similar condensates (**Figure 3- figure supplement 1 and Figure 3- movie supplement 2**), the
217 GFP tag did not artifactually drive liquid-liquid phase separation.

218 Close examination of time-lapse data revealed that the rate of fusing and splitting decreased
219 as PCNT (854-1960) condensates coalesced (**Figure 3B and Figure 3- movie supplement 1**
220 **and 2**), suggesting that the viscosity of PCNT (854-1960) condensates increased over time. To
221 test this hypothesis, we used the Dox-inducible system to induce, track, and analyze material
222 properties of young (0-3 h old) and old (20-24 h old) GFP-PCNT (854-1960) condensates by
223 FRAP. We found that young condensates recovered fluorescence almost twice as fast as the
224 old ones (**Figure 3C**). Some young condensates recovered >100% of their initial fluorescence
225 intensity because they grew in size. These results suggest that GFP-PCNT (854-1960)
226 condensates become “hardened” over time. Such molecular aging is also reported for other
227 proteins that phase separate *in vitro*, such as SPD-5 (Woodruff et al., 2017), FUS (Patel et al.,
228 2015), hnRNPA1 (Lin et al., 2015), and Tau (Wegmann et al., 2018).

229 **GFP-PCNT (854-1960) condensates selectively recruit endogenous PCM components**

230 Because the "hardened" SPD-5 condensates recruit tubulins and factors involved in MT
231 nucleation *in vitro* (Woodruff et al., 2017), we tested whether GFP-PCNT (854-1960)
232 condensates can also recruit PCM components, including structural polypeptides and "client"
233 proteins, which are also recruited to mitotic PCM (e.g., dynein and PLK1). We found that
234 endogenous PCNT, γ-tubulin, CEP215, CEP192, dynein intermediate chains (ICs), and PLK1
235 were significantly enriched in GFP-PCNT (854-1960) condensates, whereas the non-PCM
236 component ribosomal protein S6 (RPS6) was excluded (**Figure 4**). Interestingly, these recruited
237 proteins were nonuniformly distributed, with reticular patterns that resemble mitotic PCM (Lawo
238 et al., 2012; Sonnen et al., 2012). To exclude the possibility that any phase-separated
239 condensates could recruit PCM components, we examined the enrichment of PCM components
240 in the condensates formed by HOTags, the *de novo*-designed homo-oligomeric coiled-coils
241 (Grigoryan et al., 2011; Huang et al., 2014; Thomson et al., 2014), which phase separate
242 through multivalent interactions (Zhang et al., 2018). We found that PCM components γ-tubulin,
243 PCNT, and CEP192 were not enriched in the HOTag condensates (**Figure 4- figure**
244 **supplement 1**). Collectively, these results indicate that PCNT (854-1960) condensates possess
245 a unique material property that enables them to selectively recruit endogenous PCM
246 components.

247

248 **GFP-PCNT (854-1960) condensates nucleate microtubules in cells**

249 Since PCNT (854-1960) condensates recruit γ-tubulin (**Figure 4**), the protein that plays a
250 central role in MT nucleation (Felix et al., 1994; Hannak et al., 2002; Joshi et al., 1992; Oakley
251 et al., 1990; Stearns et al., 1991; Stearns & Kirschner, 1994; Zheng et al., 1991), we tested
252 whether these condensates can also nucleate MTs in cells by performing a MT renucleation

253 assay (Jao et al., 2017; Sanders et al., 2017). In this assay, we treated cells with nocodazole to
254 depolymerize MTs, washed out the drug, and monitored renucleation of MTs by anti-α-tubulin
255 immunostaining. We found that MTs were renucleated not only from the centrosome as
256 expected, but also from the interior and surface of PCNT condensates (**Figure 5A, arrows**).
257 The condensates also recruited endogenous PCNT as observed before. Some small PCNT
258 condensates also recruited endogenous PCNT and nucleated MTs (**Figure 5B, inlets,**
259 **asterisks**). Quantification of MT density in condensates and their surrounding cytoplasm
260 confirmed that PCNT condensates have a significantly higher MT renucleation activity than the
261 surrounding cytoplasm (**Figure 5C**). A similar MT renucleation assay was also performed in live
262 cells, where EB3-tdTomato was used to track the growing MT plus ends. Live cell imaging
263 showed that some PCNT condensates nucleated MTs as EB3-tdTomato signals were
264 emanating from the surface of the PCNT condensates (**Figure 5- figure supplement 1**). From
265 these two MT renucleation assays, we conclude that GFP-PCNT (854-1960) condensates
266 possess the centrosome-like MT nucleation activity in cells.

267 **Discussion**

268 Our work shows that endogenously expressed PCNT, a core PCM protein important for
269 centrosome maturation, forms liquid-like granules before incorporating into mitotic centrosomes
270 in human cells. These PCNT granules are likely formed through liquid-liquid phase separation
271 because (1) they are sensitive to the acute hexanediol treatment that is known to disrupt phase-
272 separated condensates (Kroschwald et al., 2017; Larson et al., 2017; So et al., 2019; Strom et
273 al., 2017) and (2) the coiled-coil/LCR-rich portion of PCNT undergoes concentration-dependent
274 condensation *in cellulo* that obeys characteristics of phase separation, including a sharp phase
275 transition boundary, condensate coalescence, deformability, and fast recovery in FRAP
276 experiments. Recent theoretical modeling (Zwicker et al., 2014) and *in vitro* reconstitution
277 studies (Woodruff et al., 2017) suggest that liquid-liquid phase separation underlies centrosome
278 assembly in *C. elegans*. To our knowledge, our study provides the first *in cellulo* evidence to
279 support such a model and suggests that phase separation may also underlie the assembly of
280 vertebrate centrosomes with at least one protein, PCNT, directly involved in this process.
281

282 **Is co-translational targeting of PCNT linked to its condensation during early mitosis?**

283 The liquid-like PCNT granules are predominantly observed during early mitosis when co-
284 translational targeting of PCNT to the centrosome peaks (Sepulveda et al., 2018). This raises
285 an intriguing question of whether co-translational targeting facilitates PCNT phase separation. In
286 the co-translational targeting model, multiple nascent PCNT polypeptides emerge from each
287 polysome complex with a single large *PCNT* mRNA and are transported along the MT tracks.
288 This process could effectively bring multiple N-terminal, phase separation-driving PCNT
289 polypeptides in close proximity. A proximity-driven phase separation can thus be envisioned
290 since phase separation is a concentration-dependent process. This also explains why these

291 liquid-like PCNT granules are observed predominantly during early mitosis when PCNT
292 production is maximized. This proximity-driven phase separation model is also consistent with
293 the results that phase separation of the N-terminal (2-1960) or middle (854-1960) segment of
294 PCNT can be recapitulated in the cytoplasm in a concentration-dependent manner, when it was
295 expressed exogenously and has reached its critical concentration.
296

297 **Functional significance of liquid-like PCNT granules**

298 What is the functional significance of PCNT condensation? Would it facilitate the
299 centrosomal targeting and incorporation of PCNT? Or more broadly, is the formation of liquid-
300 like PCNT granules a prerequisite for proper centrosome assembly? Woodruff and colleagues
301 show that in the presence of crowding reagents, purified centrosomal protein SPD-5 forms
302 liquid-like spherical condensates *in vitro*, which then rapidly "mature" into a gel- or solid-like
303 state (Woodruff et al., 2017). Strikingly, only these spherical SPD-5 condensates can nucleate
304 MTs, but not the solid-like SPD-5 scaffolds formed in the absence of crowding reagents
305 (Woodruff et al., 2017; Woodruff et al., 2015). Their data thus suggest that formation of a
306 condensate with liquid-like properties, even only transiently, might be important to allow
307 centrosomal proteins to be properly assembled to organize MTs (Raff, 2019; Woodruff et al.,
308 2017). A similar scenario could happen here; the formation of liquid-like PCNT granules may
309 enable the proper assembly of the human centrosome to organize MTs, for example, by
310 allowing various PCM components to "morph" into the desired configuration (also see below).
311 Important future studies are to investigate whether other PCM components are co-condensed
312 with PCNT granules, and to rationally design phase separation-deficient (and -rescuing) PCNT
313 variants to determine the significance of phase separation *per se* in centrosome function under
314 physiologically relevant conditions.

315 **Is there a liquid-to-gel/solid-like transition in PCM assembly?**

316 PCNT (854-1960) condensates transition from liquid- to gel/solid-like state, resulting in a
317 scaffold with an inhomogeneous, porous appearance (**Figures 3 and 4**). Morphologically, this
318 pattern resembles that of salt-stripped mitotic centrosomes purified from flies and clams in early
319 electron tomography studies (Moritz, Braunfeld, Fung, et al., 1995; Schnackenberg et al., 1998),
320 in which the PCM is shown as a fibrous, solid-like scaffold surrounding the centrioles. Moritz
321 and colleagues further demonstrate that upon adding bovine or fly tubulins, MTs regrow from
322 the PCM of the salt-stripped centrosomes, with MT nucleation sites distributed throughout the
323 PCM and MTs oriented in different directions (Moritz, Braunfeld, Fung, et al., 1995).
324 Interestingly, in our MT renucleation assays, we also observed a similar MT renucleation pattern
325 in the PCNT condensate; MTs were nucleated throughout the condensate and regrown into
326 different directions (**Figure 5 and Figure 5- figure supplement 1**). We thus speculate that
327 without the C-terminal PACT motif for centrosomal anchoring, the PCNT (854-1960) condensate
328 is allowed to grow freely in the cytoplasm (through the process of liquid-liquid phase
329 separation), eventually becoming a giant ensemble that shares a similar internal organization
330 with the real PCM. The similarity in organization between PCNT condensates and purified PCM
331 scaffolds implicates that centrosome assembly may be guided by a similar underlying principle,
332 pivoting on liquid-to-gel/solid-like phase transition.

333 What could be the advantage of assembling the centrosome through a liquid-to-gel/solid-like
334 transition? We speculate that with the liquid-like state (even just transiently), large scaffold
335 proteins such as PCNT, along with other PCM components, are allowed to establish the
336 interconnection before transitioning into the mature, gel/solid-like state. This “extra transitioning
337 step” might be particularly important in forming large, micron-sized, membraneless structures
338 such as the PCM.

339 **How is PCNT (854-1960) capable of recruiting endogenous PCM components and**
340 **nucleating MTs?**

341 It is surprising that the PCNT condensates formed by one-third of PCNT (residues 854-
342 1960) can selectively recruit endogenous centrosomal proteins and nucleate MTs *in cellulo*.
343 This region is particularly enriched with coiled-coils and LCRs (**Figure 2A**) and appears to
344 contain the sequence elements that drive phase separation. However, this region does not
345 contain the putative γ-tubulin-binding domains, which are within the first 350 amino acids of
346 human PCNT (T. C. Lin et al., 2014) (**Figure 2A**), nor the CEP215-binding domain, which is
347 mapped to the C-terminus of human PCNT (amino acids 2390-2406) (Kim & Rhee, 2014). Yet
348 both γ-tubulin and CEP215 (and several other PCM proteins) are recruited to these
349 condensates (**Figure 4**). One explanation is that their recruitments are mediated through the
350 endogenous PCNT that is also recruited to the condensate. Another possibility is that PCNT
351 (854-1960) contains yet to be identified binding sites for these PCM components. It is also
352 possible that PCNT (854-1960) condensates gain new material properties that enable selective
353 recruitment by generating a binding environment specific for PCM components. In the future,
354 studying the PCNT (854-1960) condensates in the *PCNT* knockout cells and reconstituting
355 PCNT (854-1960) condensates *in vitro* to test their capability of recruiting PCM components
356 would help distinguish these possibilities.
357

358 **Re-evaluating the role of coiled-coils in centrosome assembly**

359 Coiled-coils are often enriched with low-complexity sequences (Romero et al., 1999). They
360 are frequently predicted to be disordered as monomers but become folded upon formation of
361 quaternary structures (coupled folding and binding) (Anurag et al., 2012; Szappanos et al.,
362 2010; Uversky et al., 2000). Due to these unique properties, coiled-coils are known to adapt

363 vast structural variations with different superhelical stabilities to exert a wide range of biological
364 functions (Grigoryan & Keating, 2008; Li et al., 2003; Rose & Meier, 2004).
365 It has long been recognized that coiled-coil proteins are enriched at the centrosome and
366 function as parts of the "centromatrix" for the recruitment of other proteins (Doxsey, 2001;
367 Salisbury, 2003; Schnackenberg & Palazzo, 1999). Recent *in vitro* reconstitution studies of the
368 coiled-coil PCM proteins SPD-5 (*C. elegans*) and Cnn (*Drosophila*) provide strong evidence to
369 support a polymer-based mechanism of PCM assembly (Feng et al., 2017; Woodruff et al.,
370 2017; Woodruff et al., 2015). However, the exact mechanism underlying this polymer-based
371 assembly is still under debate. It also remains unclear whether this model is applicable to
372 vertebrate systems (Gupta & Pelletier, 2017; Raff, 2019).
373 We found that in cultured human cells, not only endogenously expressed full-length human
374 PCNT condense into liquid-like granules, the coiled-coil-rich PCNT segments alone can also
375 phase separate to form bioactive condensates with centrosome-like activities. These findings
376 illuminate the fundamental principle of centrosome assembly and join a growing list of studies in
377 which coiled-coil-mediated phase separation participates in a variety of biological functions
378 (Fang et al., 2019; Lu et al., 2020; Vega et al., 2019; Zeng et al., 2016).
379 Importantly, coiled-coils and LCRs of human PCNT are enriched in the regions that are
380 evolutionarily conserved, suggesting that these sequence features are under natural selection to
381 preserve critical functions. We propose that PCNT is a linear multivalent protein that phase
382 separates through its conserved coiled-coils and LCRs to become spatially organized
383 condensates that scaffold PCM assembly. This process is likely initiated during its co-
384 translational targeting to the centrosome when the nascent PCNT polypeptides are in close
385 proximity in the polysome (**Figure 6**). We propose that PCNT phase separation achieves two
386 main goals. First, it concentrates PCM components and clients as the PCNT condensates
387 selectively recruit them. This will facilitate and limit the biochemical reactions that eventually

388 take place at the centrosome (e.g., MT nucleation, kinase activities). Second, it enables a liquid-
389 to-gel/solid-like transitioning process during centrosome assembly. This process provides the
390 PCM components a thermodynamically favored pathway to assemble into a micron-sized,
391 membraneless, and yet spatially organized PCM.

392 Although coiled-coils mediate other phase separation-independent activities, it is tempting to
393 speculate that coiled-coil-mediated phase separation might be widespread among other coiled-
394 coil-rich centrosomal proteins as previously suggested (Woodruff et al., 2017). Our results
395 encourage future studies to rethink the conceptional framework regarding coiled-coil proteins
396 and phase separation in centrosome assembly and to determine whether a unified mechanism
397 is applied across metazoans.

398 **Materials and Methods**

399 **Key resources table**

Reagent type	Reagent	Source	Cat. No	Additional information
Chemical compound, drug	1,6-Hexanediol	Sigma-Aldrich, St. Louis, MO	240117	
Chemical compound, drug	DAPI	Sigma-Aldrich, St. Louis, MO	D9542	
Chemical compound, drug	Doxycycline hyclate	Sigma-Aldrich, St. Louis, MO	D9891	
Chemical compound, drug	G418 disulfate salt	Sigma-Aldrich, St. Louis, MO	A1720	
Chemical compound, drug	Nocodazole	Sigma-Aldrich, St. Louis, MO	M1404	
Chemical compound, drug	Polybrene	Santa Cruz Biotechnology Inc., Santa Cruz, CA	SC-134220	
Chemical compound, drug	Rapamycin	LC Laboratories, Woburn, MA	R-5000	
Chemical compound, drug	RO-3306	R and D Systems, Minneapolis, MN	4181	
Chemical compound, drug	Taxol	TOCRIS Bio-Techne Corporation Minneapolis, MN	1097	
Antibody	Alexa Fluor 568 goat anti-mouse IgG [H+L]	Invitrogen, Carlsbad, CA	Invitrogen Cat# A11031, RRID: AB_144696	1:500 dilution
Antibody	Alexa Fluor 568 goat anti-rabbit IgG [H+L]	Invitrogen, Carlsbad, CA	Invitrogen Cat# A11011,	1:500 dilution

			RRID: AB_143157	
Antibody	Alexa Fluor 647 goat anti-mouse IgG [H+L]	Invitrogen, Carlsbad, CA	Invitrogen Cat# A21236, RRID: AB_2535805	1:500 dilution
Antibody	Alexa Fluor 647 goat anti-rabbit IgG [H+L]	Invitrogen, Carlsbad, CA	Invitrogen Cat# A21245, RRID: AB_2535813	1:500 dilution
Antibody	Mouse anti-alpha-tubulin	Developmental Studies Hybridoma Bank (DSHB), University of Iowa, Iowa City, IA	DSHB Cat# 12G10, RRID: AB_1157911	1:100 dilution
Antibody	Mouse anti-Dynein, 74 kDa intermediate chains, cytoplasmic, clone 74.1	EMD Millipore, Burlington, MA	EMD Millipore Cat# MAB1618, RRID: AB_2246059	1:500 dilution
Antibody	Mouse anti-hGAPDH	Developmental Studies Hybridoma Bank (DSHB), University of Iowa, Iowa City, IA	DSHB Cat# DSHB-hGAPDH-2G7, RRID: AB_2617426	1:300 dilution
Antibody	Mouse anti-PLK1	EMD Millipore, Burlington, MA	EMD Millipore Cat# 05-844, RRID: AB_310836	1:1000 dilution
Antibody	Mouse anti-p53	Abcam, Cambridge, MA	Abcam Cat# ab1101, RRID: AB_297667	1:1000 dilution
Antibody	Mouse anti-ribosomal protein S6 (C-8)	Santa Cruz Biotechnology Inc., Santa Cruz, CA	Santa Cruz Biotechnology Cat# sc-74459, RRID: AB_1129205	1:50 dilution
Antibody	Mouse anti-γ-tubulin	Sigma-Aldrich, St. Louis, MO	Sigma-Aldrich Cat# T6557, RRID: AB_477584	1:500 dilution

Antibody	Rabbit anti-CDK5RAP2 (CEP215)	EMD Millipore, Burlington, MA	EMD Millipore Cat# 06-1398, RRID: AB_11203651	1:500 dilution
Antibody	Rabbit anti-CEP192	Bethyl, Montgomery, TX	Bethyl Cat# A302-324A, RRID: AB_1850234	1:500 dilution
Antibody	Rabbit anti-PCNT N terminus	Abcam, Cambridge, MA	Abcam Cat# ab4448, RRID: AB_304461	1:1000 dilution
Commercial system or kit	Corning® 50 mL Tube Top Vacuum Filter System, 0.22 μm Pore 13.6cm² CA Membrane	Corning Inc., Corning, NY	Corning Cat# 430320	
Commercial system or kit	Lipofectamine™ 3000 Transfection Reagent	Invitrogen, Carlsbad, CA	Invitrogen Cat# L3000-008	
Commercial system or kit	Neon™ Transfection System	Invitrogen, Carlsbad, CA	MPK5000	
Commercial system or kit	Neon™ Transfection System 10 μL Kit	Invitrogen, Carlsbad, CA	MPK1096	
Cell line	HEK293T cells	A gift from Henry Ho, University of California, Davis, Davis, CA	ATCC Cat# CRL-3216, RRID: CVCL_0063	
Cell line	HeLa cells	A gift from Susan Wente, Vanderbilt University, Nashville, TN	ATCC Cat# CCL-2, RRID: CVCL_0030	
Cell line	hTERT RPE-1 cells	A gift from Irina Kaverina, Vanderbilt University, Nashville, TN	ATCC Cat# CRL-4000, RRID: CVCL_4388	
Software	Fiji (ImageJ)	Image Processing and Analysis in Java	ImageJ, RRID: SCR_002285	
Software	Fusion	Andor Technology, Belfast, UK	Andor Technology	

Software	Imaris	Bitplane, Belfast, UK	Imaris, RRID: SCR_007370	
Software	Jalview	The Barton Group, University of Dundee, Scotland, UK	Jalview, RRID: SCR_006459	
Software	Microsoft Excel	Microsoft, Redmond, WA	Microsoft Excel, RRID: SCR_016137	
Software	Prism 8	Graphpad, San Diego, CA	Graphpad Prism, RRID: SCR_002798	
Software	R	R Project for Statistical Computing	R, RRID: SCR_001905	

400

401 **Constructs**

402 To generate constructs for stable expression of GFP- or mScarlet-i-PCNT segments
403 controlled by a doxycycline-inducible promoter, each PCNT segment was first amplified by PCR
404 from the pCMV-3xFLAG-EGFP-PCNT-Myc plasmid (a kind gift from Kunsoo Rhee, Seoul
405 National University, Seoul, South Korea) (Lee & Rhee, 2011) and assembled into a vector with
406 sfGFP or mScarlet-i by Gibson assembly (Gibson et al., 2009). The final constructs with the
407 *piggyBac* transposon elements and doxycycline-inducible promoter were made by subcloning
408 the sfGFP- or mScarlet-i-PCNT fragment into PB-TA-ERN (a gift from Knut Woltjen, Addgene
409 plasmid #80474; http://n2t.net/addgene:80474; RRID: Addgene_80474) (Kim et al., 2016) using
410 the Gateway cloning system (Thermo Fisher Scientific, Waltham, MA). The following *piggyBac*
411 transposon constructs, with amino acid sequences of human PCNT in the parentheses, were
412 used in this study: PB-TA-sfGFP-PCNT (2-891), PB-TA-sfGFP-PCNT (854-1960), PB-TA-
413 sfGFP-PCNT (2-1960), and PB-TA-sfGFP-PCNT (1954-3336), PB-TA-mScarlet-i-PCNT (854-
414 1960).

415 To make the construct to label microtubule plus ends, the EB3-tdTomato fragment was
416 amplified by PCR from the EB3-tdTomato plasmid (a gift from Erik Dent, Addgene plasmid
417 #50708; http://n2t.net/addgene:50708; RRID: Addgene_50708) (Merriam et al., 2013) and
418 cloned into a lentiviral targeting plasmid pLVX-EF1α-mCherry-N1 without the mCherry portion (a
419 gift from Henry Ho, 631986, Takara Bio, Mountain View, CA) by Gibson assembly. The resulting
420 plasmid, pLVX-EF1α-EB3-tdTomato, was used to make lentiviruses to transduce cultured
421 human cells.
422 To make the construct to label DNA, mScarlet-i-H2A construct was amplified by PCR from
423 the pmScarlet-i_H2A_C1 plasmid (a gift from Dorus Gadella, Addgene plasmid #85053;
424 http://n2t.net/addgene:85053; RRID: Addgene_85053) (Bindels et al., 2017) and cloned into the
425 same lentiviral targeting construct by Gibson assembly as described above to generate pLVX-
426 EF1α-mScarlet-i-H2A.
427 To make the construct to label the centrioles with far red fluorescence, the coding sequence
428 of human centrin 2 (CETN2) was first cloned from total RNA of HEK293T cells using the
429 SuperScript® III One-Step RT-PCR System (Invitrogen). The miRFP670 was amplified by PCR
430 from the pmiRFP670-N1 plasmid (a gift from Vladislav Verkhusha, Addgene plasmid #79987;
431 http://n2t.net/addgene:79987; RRID: Addgene_79987) (Shcherbakova et al., 2016). miRFP670
432 and CETN2 were then assembled into the same lentiviral targeting construct by Gibson
433 assembly as described above to generate pLVX-EF1α-miRFP670-CETN2.
434 To generate the Cas9 tagged with the nuclear localization signal (NLS) at both the N- and
435 C-termini for expression in mammalian cells, an NLS from SV40 large T-antigen (Kalderon et
436 al., 1984) was synthesized and added to hCas9, a construct encoding a human codon-
437 optimized Cas9 (hCas9) with an NLS at its C-terminus (a gift from George Church, Addgene
438 plasmid #41815; http://n2t.net/addgene:41815; RRID: Addgene_41815) (Mali et al., 2013), by
439 PCR. The final construct, pCMVSP6-NLS-hCas9-NLS-polyA_Tol2pA2, with NLS-hCas9-NLS

440 under the control of the cytomegalovirus (CMV) immediate-early enhancer and promoter was
441 generated by the Gateway cloning system (Thermo Fisher Scientific) using the components
442 from the Tol2kit (Kwan et al., 2007).
443

444 **Cell culture**

445 RPE-1 cells (a gift from Irina Kaverina, Vanderbilt University) were maintained in Dulbecco's
446 Modification of Eagles Medium/Ham's F-12 50/50 Mix (DMEM/F-12) (10–092-CV, Corning,
447 Corning, NY). HeLa cells (ATCC CCL-2, a gift from Susan Wente, Vanderbilt University,
448 Nashville, TN) and HEK293T cells (a gift from Henry Ho, University of California, Davis, Davis,
449 CA) were maintained in DMEM (10–017-CV, Corning). All cell lines were supplemented with
450 10% fetal bovine serum (FBS) (12303C, lot no. 13G114, Sigma-Aldrich, St. Louis, MO), 1x
451 Penicillin Streptomycin (30–002 CI, Corning), and maintained in a humidified incubator with 5%
452 CO_2 at 37°C.
453 Cell lines used in this study were not further authenticated after obtaining from the sources.
454 All cell lines were tested negative for mycoplasma using a PCR-based testing with the Universal
455 Mycoplasma Detection Kit (30–1012K, ATCC, Manassas, VA). None of the cell lines used in this
456 study was included in the list of commonly misidentified cell lines maintained by International
457 Cell Line Authentication Committee.
458

459 **Generation of GFP-PCNT knock-in cell line**

460 The CRISPR/Cas9 technology with a double-cut homology directed repair (HDR) donor was
461 used to knock in sfGFP into the *PCNT* locus of RPE-1 cells (S. Lin et al., 2014; Zhang et al.,
462 2017). Because it was unclear if knocking in sfGFP would perturb centrosome integrity that
463 might lead to p53-dependent cell cycle arrest (Mikule et al., 2007), making it unfavorable to

464 isolate the knock-in clones, we first generated a *TP53* knockout RPE-1 cell line before the
465 knock-in experiment (**Figure 1- figure supplement 3**). Knocking out *TP53* was achieved
466 through the CRISPR-mediated gene editing by co-expression of Cas9 protein with the gRNA
467 targeting *TP53* (5'-GGGCAGCTACGGTTTCCGTC-3') using the method described by the
468 Church group (Mali et al., 2013). The gRNA template was cloned into the gRNA Cloning Vector
469 (Addgene plasmid # 41824; http://n2t.net/addgene:41824; RRID: Addgene_41824) via Gibson
470 assembly. 1 μg Cas9 plasmid (pCMVSP6-NLS-hCas9-NLS-polyA_Tol2pA2) and 1 μg gRNA
471 plasmid were transfected into RPE-1 cells using the Lipofectamine P3000 reagent according to
472 the manufacturer's instruction (Invitrogen, Carlsbad, CA). Cells were expanded, isolated as
473 single colonies, and screened for frameshift mutations in both *TP53* alleles by high-throughput
474 Illumina sequencing. The loss of TP53 expression was further confirmed by Western blot
475 analysis. A *TP53*$^{-/-}$;RPE-1 cell line (RPE-1_1-1) was used in this study (**Figure 1- figure**
476 **supplement 3**).
477 To knock in sfGFP into the *PCNT* locus, crRNA/tracrRNA (i.e., the Alt-R system, Integrated
478 DNA Technologies, Coralville, IA) were used to target a sequence near the start codon of *PCNT*
479 (CGCGCGGAGTCTGAGGGAGA). The double-cut HDR donor contains the sfGFP-PCNT
480 cassette with 600-bp homology arms flanked by the same guide RNA target sequence
481 (synthesized and cloned into pUC57-Kan vector, Genewiz, South Plainfield, NJ) (**Figure 1-**
482 **figure supplement 1**). Annealed crRNA/tracrRNA and Cas9 protein (a kind gift from Fuguo
483 Jiang and Jennifer Doudna, Jiang et al., 2016; Jiang et al., 2015) were incubated in 30 mM
484 HEPES, pH 7.5, 1 mM $MgCl_2$, 200 mM KCl, and 1 mM TCEP at 37°C for 10 min to form the
485 Cas9 ribonucleoprotein (RNP) complexes. Before electroporation, the HDR donor plasmid was
486 mixed with 2 x 10^5 of the *TP53*$^{-/-}$;RPE-1 cells synchronized to early M phase using RO-3306 as
487 done before (Sepulveda et al., 2018). The Cas9 RNP complexes were then mixed with the
488 cell/donor vector mix, followed by electroporation using the Neon electroporation system with a

489 10-μl tip according to the manufacturer's instruction (Pulse voltage: 1200 V, pulse width: 25,
490 pulse number: 4, Invitrogen). The final concentrations of the annealed crRNA/tracrRNA, Cas9
491 protein, and HDR donor plasmid are 3 μM, 2 μM, and 120 nM, respectively, in a total volume of
492 10 μl. After electroporation, the cells were grown for 10-14 days in dilute density. Individual
493 clones were isolated and screened for the presence of GFP-positive centrosomes. The GFP-
494 positive clones were further confirmed by anti-PCNT immunostaining and sequencing the
495 junctions of the sfGFP integration site (primer sequences are in **Supplementary file 1**).
496

497 **Generation of doxycycline-inducible cell lines with GFP- or mScarlet-i-PCNT segments**

498 We used a previously described *piggyBac* transposon system (Kim et al., 2016) to generate
499 stable cell lines that express different GFP- or mScarlet-i-PCNT fusions in a doxycycline-
500 inducible manner. In brief, the PB-TA-sfGFP-PCNT or PB-TA-mScarlet-i-PCNT *piggyBac*
501 transposon construct and a *piggyBac* transposase plasmid (PB210PA-1, System Biosciences,
502 Palo Alto, CA) were electroporated into *TP53*$^{-/-}$;RPE-1 cells using the Neon electroporation
503 system according to the manufacturer's instruction (Invitrogen). After 8-10 day of 200 mg/ml
504 G418 treatment, sfGFP-PCNT integrated cells were obtained. Sometimes fluorescence
505 activated cell sorting (FACS) was further performed to obtain cells with desired, more uniform
506 expression levels of fusion proteins.
507

508 **Generation of stable cell lines by lentiviral transduction**

509 To generate recombinant lentiviruses expressing EB3-tdTomato, pLVX-EF1α-EB3-tdTomato
510 plasmid was first co-transfected with the following third-generation packaging plasmids (gifts
511 from Didier Trono): pMD2.G (Addgene plasmid #12259; http://n2t.net/addgene:12259; RRID:
512 Addgene_12259), pRSV-rev (Addgene plasmid #12253; http://n2t.net/addgene:12253; RRID:

513 Addgene_12253), and pMDLg/pRRE (Addgene plasmid #12251; http://n2t.net/addgene:12251;
514 RRID: Addgene_12251) (Dull et al., 1998) into HEK293T cells. Viral supernatants were
515 collected from media 24-48 h post transfection, filtered by a 0.22-μm filter, and were used to
516 infect the inducible GFP-PCNT (854-1960) *TP53*$^{-/-}$;RPE-1 cells with 8 μg/ml polybrene. 18-24 h
517 post infection, the viruses were removed and the cells were expanded. To minimize the impact
518 on microtubule dynamics, the cells expressing low levels of EB3-tdTomato (gated and collected
519 by FACS) were used for experiments.
520 To generate lentiviruses expressing mScarlet-i-H2A and miRFP670-CETN2, the same
521 procedure was performed as above except for using the targeting vectors pLVX-EF1α-mScarlet-
522 i-H2A and pLVX-EF1α-miRFP670-CETN2, respectively. The resulting viral supernatants were
523 used to infect the GFP-PCNT knock-in cells as described above.
524

525 **Measurement of protein enrichment in PCNT and HOTag condensates**

526 To test whether the PCNT condensates recruit PCM but exclude non-PCM components,
527 about 5 x 10^4 GFP-PCNT (854-1960) cells were seeded onto each 12-mm circular coverslip in a
528 24-well plate, treated with 1 μg/ml doxycycline treatment for 24 h, followed by immunostaining.
529 To compare the recruitment of PCM component between the PCNT and non-PCNT
530 condensates, the HOTag3/6 condensates (Zhang et al., 2018) were formed by transfecting
531 pcDNA3-FKBP-EGFP-HOTag3 and pcDNA3-Frb-EGFP-HOTag6 plasmids (gifts from Xiaokun
532 Shu; Addgene plasmid #106924 and #106919, respectively) into *TP53*$^{-/-}$;RPE-1 cells using the
533 Lipofectamine P3000 reagent according to the manufacturer's instruction (Invitrogen). In
534 parallel, the doxycycline-inducible GFP-PCNT (854-1960) cells were treated with 1 μg/ml
535 doxycycline for 6 h to induce the formation of PCNT condensates. Cells with either HOTag or

536 PCNT condensates were then treated with 100 nM rapamycin for 1 h (to induce the formation of
537 HOTag condensates) prior to immunostaining.
538

539 **Microtubule renucleation assay**

540 Microtubule renucleation assay was adapted from previous studies (Jao et al., 2017;
541 Sanders et al., 2017). In brief, cells were treated with 8.3 μM nocodazole for 2 h to depolymerize
542 microtubules. The plate containing the treated cells was then placed on ice, while washing the
543 cells with ice-cold media for 8 times to remove nocodazole. To allow microtubules to renucleate,
544 the plate was then placed in a 37°C water bath while the cells were incubated with pre-warmed
545 media for 65-110 s (the optimal regrowth period varied between experiments), followed by a 10-
546 s incubation with pre-warmed Extraction Buffer (60 mM PIPES, pH 6.9, 25 mM HEPES, 10 mM
547 EGTA, 2 mM $MgCl_2$, 0.1% Saponin, 0.25 nM nocodazole, 0.25 nM taxol). Immediately after the
548 regrowth, the cells were fixed with 4% paraformaldehyde, 0.025% glutaraldehyde in
549 Cytoskeleton Buffer (10 mM MES, 150 mM NaCl, 5 mM $MgCl_2$, 5 mM EGTA, 5 mM D-glucose)
550 for 10 min at room temperature. The cells were then incubated with 0.2% $NaBH_4$ in 1x PBS for
551 10 min at room temperature to quench the autofluorescence before immunostaining. For the live
552 MT renucleation assay, the nocodazole-treated EB3-tdTomato-expressing cells with PCNT
553 condensates were mounted on the microscope stage, first imaged in the presence of
554 nocodazole, followed by washes with pre-warmed fresh media 5 times. After washes, the cells
555 were imaged again at 1-min intervals to monitor MT renucleation.
556

557 **Immunostaining**

558 Immunostaining was performed as previously described (Jiang et al., 2019; Sepulveda et
559 al., 2018). In brief, cells were fixed for 15 min in 4% paraformaldehyde in 1x PBS at room

560 temperature or 5 min in ice-cold 100% methanol at -20°C. Cells were then washed twice with 1x
561 PBS and incubated with Blocking Solution (2% goat serum, 0.1% Triton X-100, and 10 mg/ml
562 bovine serum albumin in 1x PBS) for 1 h at room temperature. Cells were then incubated with
563 Blocking Solution containing diluted primary antibody for 1 h at room temperature, washed three
564 times with 1x PBS, and incubated with Blocking Solution containing diluted secondary antibody
565 for 1 hr at room temperature. Cells were washed three times with 1x PBS, and nuclei were
566 counterstained with 0.05 mg/ml DAPI in 1x PBS for 30 min at room temperature before
567 mounting.
568

569 **Microscopy**

570 Confocal microscopy was performed using a spinning disk confocal microscope system
571 (Dragonfly, Andor Technology, Belfast, UK) housed within a wrap-around incubator (Okolab,
572 Pozzuoli, Italy) with Leica 63x/1.40 or 100x/1.40 HC PL APO objectives, an iXon Ultra 888
573 EMCCD camera, or a Zyla sCMOS camera for immunofluorescence and live cell imaging.
574 Deconvolution was performed using the Fusion software (Andor Technology).
575 For live imaging, cells were seeded in 35-mm glass-bottom dishes 12-18 h prior to imaging
576 and were imaged in a humidified environmental chamber with 5% CO_2 at 37°C.
577 For acute 1,6-hexanediol treatment, 3.5% 1,6-hexanediol in 10% FBS DMEM/F-12 media
578 was added 2 min after the start of time-lapse imaging at 37°C (every 3 min for 5 times; time 0 =
579 the time 1,6-hexanediol was added). Control cells (i.e., no 1,6-hexanediol) were imaged in
580 parallel under the same acquisition condition and intervals.

581 **Fluorescence recovery after photobleaching (FRAP)**

582 A FRAP photoablation module with a computer-controlled fiber optically pumped dye laser
583 was used to bleach a region-of-interest (ROI) on the condensate (~2 μm in diameter) after a few
584 pre-bleach images were acquired. After photobleaching, the same ROI continued to be imaged
585 at 2-s (young condensates) or 5-s (old condensates) intervals for 5 to 12 min. Images were
586 acquired using a Zeiss AxioObserver with a 60x objective coupled with a Yokogawa CSU-10
587 spinning disk confocal system and a Photometrics CoolSNAP HQ2 cooled CCD camera
588 (BioImaging Solutions, San Diego, CA). The microscope system was controlled by Slidebook
589 software (Intelligent Imaging Innovations, Denver, CO) and was enclosed in an environmental
590 chamber with temperature set at 37°C. Images and data were analyzed using ImageJ, Microsoft
591 Excel, and GraphPad Prism 8 (GraphPad, San Diego, CA).

592

593 **Measurement of relative protein concentrations in cells**

594 Doxycycline-inducible cell lines expressing individual GFP-PCNT segments were seeded on
595 glass-bottom 35-mm dishes and live imaging started after addition of 1 μg/ml doxycycline.
596 Imaging of different cell lines was performed with the same acquisition setting and condition (5%
597 CO_2 at 37°C) using a spinning disk confocal microscope system (Dragonfly, Andor Technology).
598 To estimate the relative protein concentrations of GFP-PCNT in cells, the volumes of the
599 condensates and their surrounding cytoplasm were first determined from the confocal voxels.
600 This was done by performing surface rendering of the GFP signals of the condensates (dense
601 phase) and of the whole cytoplasm (light phase) with different thresholds using the Surface
602 reconstruction function of Imaris (Bitplane, Belfast, UK). Depending on the GFP expression level
603 in each cell, threshold values were manually selected for rendering. The volume and intensity
604 sums of each rendered surface were then calculated. The volume and intensity sums in the light

605 (cytoplasm) phase were calculated by subtracting the values in the dense phase from the total
606 in the cell. Relative protein concentrations were calculated as intensity sum per volume. The
607 critical concentration of phase-separated PCNT segments was determined as the cytoplasmic
608 protein concentration (light phase) of the phase-separated cells since this value stayed relatively
609 constant once the protein phase separated in cells.
610

611 **Quantification of protein intensity in the condensates**

612 To quantify the fold enrichment of various proteins in the condensates, three randomly
613 chosen fixed areas in the condensates and in the cytoplasm per cell (2.25 μm^2 for data in
614 **Figure 4**, 0.159 μm^2 for data in **Figure 4- figure supplement 1**) were selected for quantification
615 using Fiji. The mean protein intensity value in each selected area was exported into an Excel
616 sheet. The averaged mean intensity values in the cytoplasm and in the condensates per cell
617 were calculated. The fold enrichment in the condensates is calculated as the ratio of protein
618 intensity mean in the condensates per cell to the overall protein intensity mean in the cytoplasm.
619 For cells with centrosomes embedded in the PCNT condensates, PCM protein signals at the
620 centrosomes within the PCNT condensates were excluded from quantification.
621

622 **Quantification of microtubule density**

623 Each condensate was manually outlined as the first ROI using the freehand selection tool in
624 Fiji. The second ROI was then defined as the cytoplasm space between the outline of the first
625 ROI and the outline 1 μm larger than the first ROI. Values of area and intensity sum of anti-α-
626 tubulin signals in the first (condensate) and second (cytoplasm) ROIs were then calculated in an
627 Excel sheet. One or two condensates was quantified per cell. Microtubule density was
628 calculated as anti-α-tubulin intensity sum per area. Normalized microtubule density was

629 calculated as the ratio of microtubule density in the condensate to the averaged microtubule
630 density in the cytoplasm.
631

632 **Multiple protein sequence alignments**

633 Protein sequences of pericentrin orthologs from a diverse group of vertebrates, as well as
634 two functional homologs of pericentrin from budding yeast (Spc110) and fruit fly (pericentrin-like
635 protein, D-Plp), were retrieved from Ensembl genome database (http://uswest.ensembl.org),
636 resulting in a total of 233 sequences. We further filtered sequences to eliminate those with low-
637 quality sequence reads, incomplete annotations, and those inducing large gaps (e.g., due to the
638 insertions specific to small numbers of species), resulting in a final list of 169 sequences. These
639 169 sequences were then aligned using MUSCLE (Edgar, 2004) and colored with the default
640 Clustal X color scheme in Jalview (**Figure 2- table 1**) (Waterhouse et al., 2009). The
641 conservation of each residue was scored using the AMAS method of multiple sequence
642 alignment analysis in Jalview (Livingstone & Barton, 1993).
643

644 **Statistical analysis**

645 Statistical analysis was performed using the GraphPad Prism 8 (GraphPad). Each sample
646 size (n value) is indicated in the corresponding figure or figure legend. Significance was
647 assessed by performing an unpaired two-sided Student's t-test, as indicated in individual
648 figures. The experiments were not randomized. The investigators were not blinded to allocation
649 during experiments and outcome assessment.

650 **Acknowledgement**

651 We thank Dr. Bo Huang for discussion with the CRISPR knock-in strategy; Dr. Kunsoo Rhee
652 for human PCNT cDNA; Dr. Rick McKenney for the sfGFP construct; Dr. Henry Ho for HEK293T
653 cells, pLVX-EF1α-mCherry-N1, lentiviral packaging plasmids, and critical reading of the
654 manuscript; Dr. Susan Wente for HeLa cells; Dr. Irina Kaverina for RPE-1 cells; Drs. Fuguo
655 Jiang and Jennifer Doudna for Cas9 protein; Dr. Megan Dennis for analyzing Illumina
656 sequencing results; Linhao Jiang for data processing, programming, and analysis of multiple
657 alignment data; Stephen (Evan) Brahms, Marvin Orellana, Hashim Shaikh, Janice Tam, and
658 Alan Zhong for technical help with cell culture work; all members of the Jao and Ho labs for
659 discussion; Emily Jao for help with illustration of the model figure. Experiments were performed
660 in part through the use of Davis Campus Shared Flow Cytometry Resource. The article is
661 dedicated to the memory of Dr. Fuguo Jiang, who recently passed away. Fuguo purified the
662 Cas9 protein and kindly shared it with us for this study.

663 **Legends for movie supplements**

664 **Figure 1- movie supplement 1. A time-lapse movie of a GFP-PCNT knock-in cell.** Part of
665 the time-lapse micrographs (inset #1) are shown in Example 1 of Figure 1. Arrowheads denote
666 the fusing and splitting events of the GFP-PCNT granules. Asterisks denote the centrosomes.
667

668 **Figure 1- movie supplement 2. A time-lapse movie of a GFP-PCNT knock-in cell.** Part of
669 the time-lapse micrographs (inset #1) are shown in Example 2 of Figure 1. Arrowheads denote
670 the fusing and splitting events of the GFP-PCNT granules. Asterisks denote the centrosomes.
671

672 **Figure 1- movie supplement 3. A time-lapse movie of a GFP-PCNT knock-in cell from**
673 **another independent knock-in clone.** Asterisks denote the centrosomes. Note the fusing and
674 splitting events of the GFP-PCNT granules near centrosomes.
675

676 **Figure 2- movie supplement 1. Time-lapse movie of GFP-PCNT (2-1960) condensates in**
677 **RPE-1 cells 24 h post Dox induction.** Part of the time-lapse micrographs (inset #1) are shown
678 in Figure 2C.
679

680 **Figure 2- movie supplement 2. Time-lapse movie of GFP-PCNT (1954-3336) solid-like**
681 **scaffolds in RPE-1 cells 24 h post Dox induction.** Part of the time-lapse micrographs (inset
682 #1) are shown in Figure 2C.
683

684 **Figure 3- movie supplement 1. Time-lapse movie of GFP-PCNT (854-1960) in RPE-1 cells.**
685 Time-lapse imaging started 3.5 h post Dox induction. The centrosomes are labeled by

686 miRFP670-CETN2 fusion protein. Part of the time-lapse micrographs are shown in Figure 3B.

687 GFP-PCNT (854-1960) in yellow, miRFP670-CETN2 in magenta.

688

689 **Figure 3- movie supplement 2. Time-lapse movie of mScarlet-i-PCNT (854-1960) in RPE-1**

690 **cells.** In some cells, the centrosomes are labeled by miRFP670-CETN2 fusion protein.

691 mScarlet-i-PCNT (854-1960) in cyan, miRFP670-CETN2 in magenta.

692 **References**

693

694 Alvarez-Rodrigo, I., Steinacker, T. L., Saurya, S., Conduit, P. T., Baumbach, J., Novak, Z. A.,
695 Aydogan, M. G., Wainman, A., & Raff, J. W. (2019, Sep 9). Evidence that a positive
696 feedback loop drives centrosome maturation in fly embryos. *Elife, 8*, DOI:
697 10.7554/eLife.50130. https://doi.org/10.7554/eLife.50130
698

699 Andersen, J. S., Wilkinson, C. J., Mayor, T., Mortensen, P., Nigg, E. A., & Mann, M. (2003, Dec
700 4). Proteomic characterization of the human centrosome by protein correlation profiling.
701 *Nature, 426*(6966), 570-574. https://doi.org/10.1038/nature02166
702

703 Anitha, A., Nakamura, K., Yamada, K., Iwayama, Y., Toyota, T., Takei, N., Iwata, Y., Suzuki, K.,
704 Sekine, Y., Matsuzaki, H., Kawai, M., Thanseem, I., Miyoshi, K., Katayama, T., Matsuzaki,
705 S., Baba, K., Honda, A., Hattori, T., Shimizu, S., Kumamoto, N., Kikuchi, M., Tohyama, M.,
706 Yoshikawa, T., & Mori, N. (2009, Oct 05). Association studies and gene expression analyses
707 of the DISC1-interacting molecules, pericentrin 2 (PCNT2) and DISC1-binding zinc finger
708 protein (DBZ), with schizophrenia and with bipolar disorder. *Am J Med Genet B*
709 *Neuropsychiatr Genet, 150B*(7), 967-976. https://doi.org/10.1002/ajmg.b.30926
710

711 Anurag, M., Singh, G. P., & Dash, D. (2012, Jan). Location of disorder in coiled coil proteins is
712 influenced by its biological role and subcellular localization: a GO-based study on human
713 proteome. *Mol Biosyst, 8*(1), 346-352. https://doi.org/10.1039/c1mb05210a
714

715 Asherie, N. (2004, Nov). Protein crystallization and phase diagrams. *Methods, 34*(3), 266-272.
716 https://doi.org/10.1016/j.ymeth.2004.03.028
717

718 Atkins, J. D., Boateng, S. Y., Sorensen, T., & McGuffin, L. J. (2015, Aug 13). Disorder Prediction
719 Methods, Their Applicability to Different Protein Targets and Their Usefulness for Guiding
720 Experimental Studies. *Int J Mol Sci, 16*(8), 19040-19054.
721 https://doi.org/10.3390/ijms160819040
722

723 Banani, S. F., Lee, H. O., Hyman, A. A., & Rosen, M. K. (2017, May). Biomolecular
724 condensates: organizers of cellular biochemistry. *Nat Rev Mol Cell Biol, 18*(5), 285-298.
725 https://doi.org/10.1038/nrm.2017.7
726

727 Barr, A. R., & Gergely, F. (2007, Sep 1). Aurora-A: the maker and breaker of spindle poles. *J*
728 *Cell Sci, 120*(Pt 17), 2987-2996. https://doi.org/10.1242/jcs.013136
729

730 Berdnik, D., & Knoblich, J. A. (2002, Apr 16). Drosophila Aurora-A is required for centrosome
731 maturation and actin-dependent asymmetric protein localization during mitosis. *Curr Biol,*
732 *12*(8), 640-647. https://doi.org/10.1016/s0960-9822(02)00766-2
733

734 Berry, J., Weber, S. C., Vaidya, N., Haataja, M., & Brangwynne, C. P. (2015, Sep 22). RNA
735 transcription modulates phase transition-driven nuclear body assembly. *Proc Natl Acad Sci*
736 *U S A, 112*(38), E5237-5245. https://doi.org/10.1073/pnas.1509317112
737

738 Bindels, D. S., Haarbosch, L., van Weeren, L., Postma, M., Wiese, K. E., Mastop, M., Aumonier,
739 S., Gotthard, G., Royant, A., Hink, M. A., & Gadella, T. W., Jr. (2017, Jan). mScarlet: a

740 bright monomeric red fluorescent protein for cellular imaging. *Nat Methods, 14*(1), 53-56.
741 https://doi.org/10.1038/nmeth.4074
742
743 Boeynaems, S., Alberti, S., Fawzi, N. L., Mittag, T., Polymenidou, M., Rousseau, F.,
744 Schymkowitz, J., Shorter, J., Wolozin, B., Van Den Bosch, L., Tompa, P., & Fuxreiter, M.
745 (2018, Jun). Protein Phase Separation: A New Phase in Cell Biology. *Trends Cell Biol,*
746 *28*(6), 420-435. https://doi.org/10.1016/j.tcb.2018.02.004
747
748 Boke, E., Ruer, M., Wuhr, M., Coughlin, M., Lemaitre, R., Gygi, S. P., Alberti, S., Drechsel, D.,
749 Hyman, A. A., & Mitchison, T. J. (2016, Jul 28). Amyloid-like Self-Assembly of a Cellular
750 Compartment. *Cell, 166*(3), 637-650. https://doi.org/10.1016/j.cell.2016.06.051
751
752 Conduit, P. T., Brunk, K., Dobbelaere, J., Dix, C. I., Lucas, E. P., & Raff, J. W. (2010, Dec 21).
753 Centrioles regulate centrosome size by controlling the rate of Cnn incorporation into the
754 PCM. *Curr Biol, 20*(24), 2178-2186. https://doi.org/10.1016/j.cub.2010.11.011
755
756 Conduit, P. T., Feng, Z., Richens, J. H., Baumbach, J., Wainman, A., Bakshi, S. D., Dobbelaere,
757 J., Johnson, S., Lea, S. M., & Raff, J. W. (2014, Mar 31). The centrosome-specific
758 phosphorylation of Cnn by Polo/Plk1 drives Cnn scaffold assembly and centrosome
759 maturation. *Dev Cell, 28*(6), 659-669. https://doi.org/10.1016/j.devcel.2014.02.013
760
761 Conduit, P. T., Richens, J. H., Wainman, A., Holder, J., Vicente, C. C., Pratt, M. B., Dix, C. I.,
762 Novak, Z. A., Dobbie, I. M., Schermelleh, L., & Raff, J. W. (2014, Aug 22). A molecular
763 mechanism of mitotic centrosome assembly in Drosophila. *Elife, 3*, e03399.
764 https://doi.org/10.7554/eLife.03399
765
766 Conduit, P. T., Wainman, A., & Raff, J. W. (2015, Oct). Centrosome function and assembly in
767 animal cells. *Nat Rev Mol Cell Biol, 16*(10), 611-624. https://doi.org/10.1038/nrm4062
768
769 Delaval, B., & Doxsey, S. J. (2010, Jan 25). Pericentrin in cellular function and disease. *J Cell*
770 *Biol, 188*(2), 181-190. https://doi.org/10.1083/jcb.200908114
771
772 Dobbelaere, J., Josue, F., Suijkerbuijk, S., Baum, B., Tapon, N., & Raff, J. (2008, Sep 16). A
773 genome-wide RNAi screen to dissect centriole duplication and centrosome maturation in
774 Drosophila. *PLoS Biol, 6*(9), e224. https://doi.org/10.1371/journal.pbio.0060224
775
776 Dosztanyi, Z., Csizmok, V., Tompa, P., & Simon, I. (2005, Apr 8). The pairwise energy content
777 estimated from amino acid composition discriminates between folded and intrinsically
778 unstructured proteins. *J Mol Biol, 347*(4), 827-839. https://doi.org/10.1016/j.jmb.2005.01.071
779
780 Doxsey, S. (2001, Sep). Re-evaluating centrosome function. *Nat Rev Mol Cell Biol, 2*(9), 688-
781 698. https://doi.org/10.1038/35089575
782
783 Dull, T., Zufferey, R., Kelly, M., Mandel, R. J., Nguyen, M., Trono, D., & Naldini, L. (1998, Nov).
784 A third-generation lentivirus vector with a conditional packaging system. *J Virol, 72*(11),
785 8463-8471. https://www.ncbi.nlm.nih.gov/pubmed/9765382
786
787 Edgar, R. C. (2004). MUSCLE: multiple sequence alignment with high accuracy and high
788 throughput. *Nucleic Acids Res, 32*(5), 1792-1797. https://doi.org/10.1093/nar/gkh340

789
790 Elbaum-Garfinkle, S., Kim, Y., Szczepaniak, K., Chen, C. C., Eckmann, C. R., Myong, S., &
791 Brangwynne, C. P. (2015, Jun 9). The disordered P granule protein LAF-1 drives phase
792 separation into droplets with tunable viscosity and dynamics. *Proc Natl Acad Sci U S A,*
793 *112*(23), 7189-7194. https://doi.org/10.1073/pnas.1504822112
794
795 Fang, X., Wang, L., Ishikawa, R., Li, Y., Fiedler, M., Liu, F., Calder, G., Rowan, B., Weigel, D.,
796 Li, P., & Dean, C. (2019, May). Arabidopsis FLL2 promotes liquid-liquid phase separation of
797 polyadenylation complexes. *Nature, 569*(7755), 265-269. https://doi.org/10.1038/s41586-
798 019-1165-8
799
800 Felix, M. A., Antony, C., Wright, M., & Maro, B. (1994, Jan). Centrosome assembly in vitro: role
801 of gamma-tubulin recruitment in Xenopus sperm aster formation. *J Cell Biol, 124*(1-2), 19-
802 31. https://doi.org/10.1083/jcb.124.1.19
803
804 Feng, Z., Caballe, A., Wainman, A., Johnson, S., Haensele, A. F. M., Cottee, M. A., Conduit, P.
805 T., Lea, S. M., & Raff, J. W. (2017, Jun 1). Structural Basis for Mitotic Centrosome Assembly
806 in Flies. *Cell, 169*(6), 1078-1089 e1013. https://doi.org/10.1016/j.cell.2017.05.030
807
808 Fu, J., & Glover, D. M. (2012, Aug). Structured illumination of the interface between centriole
809 and peri-centriolar material. *Open Biol, 2*(8), 120104. https://doi.org/10.1098/rsob.120104
810
811 Galati, D. F., Sullivan, K. D., Pham, A. T., Espinosa, J. M., & Pearson, C. G. (2018, Sep 10).
812 Trisomy 21 Represses Cilia Formation and Function. *Dev Cell, 46*(5), 641-650 e646.
813 https://doi.org/10.1016/j.devcel.2018.07.008
814
815 Gibson, D. G., Young, L., Chuang, R. Y., Venter, J. C., Hutchison, C. A., 3rd, & Smith, H. O.
816 (2009, May). Enzymatic assembly of DNA molecules up to several hundred kilobases. *Nat*
817 *Methods, 6*(5), 343-345. https://doi.org/10.1038/nmeth.1318
818
819 Gillingham, A. K., & Munro, S. (2000, Dec). The PACT domain, a conserved centrosomal
820 targeting motif in the coiled-coil proteins AKAP450 and pericentrin. *EMBO Rep, 1*(6), 524-
821 529. https://doi.org/10.1093/embo-reports/kvd105
822
823 Goshima, G., Wollman, R., Goodwin, S. S., Zhang, N., Scholey, J. M., Vale, R. D., & Stuurman,
824 N. (2007, Apr 20). Genes required for mitotic spindle assembly in Drosophila S2 cells.
825 *Science, 316*(5823), 417-421. https://doi.org/10.1126/science.1141314
826
827 Griffith, E., Walker, S., Martin, C. A., Vagnarelli, P., Stiff, T., Vernay, B., Al Sanna, N., Saggar,
828 A., Hamel, B., Earnshaw, W. C., Jeggo, P. A., Jackson, A. P., & O'Driscoll, M. (2008, Feb).
829 Mutations in pericentrin cause Seckel syndrome with defective ATR-dependent DNA
830 damage signaling. *Nat Genet, 40*(2), 232-236. https://doi.org/10.1038/ng.2007.80
831
832 Grigoryan, G., & Keating, A. E. (2008, Aug). Structural specificity in coiled-coil interactions. *Curr*
833 *Opin Struct Biol, 18*(4), 477-483. https://doi.org/10.1016/j.sbi.2008.04.008
834
835 Grigoryan, G., Kim, Y. H., Acharya, R., Axelrod, K., Jain, R. M., Willis, L., Drndic, M., Kikkawa,
836 J. M., & DeGrado, W. F. (2011, May 27). Computational design of virus-like protein

assemblies on carbon nanotube surfaces. *Science, 332*(6033), 1071-1076. https://doi.org/10.1126/science.1198841

Gupta, G. D., & Pelletier, L. (2017, Sep 11). Centrosome Biology: Polymer-Based Centrosome Maturation. *Curr Biol, 27*(17), R836-R839. https://doi.org/10.1016/j.cub.2017.07.036

Hamill, D. R., Severson, A. F., Carter, J. C., & Bowerman, B. (2002, Nov). Centrosome maturation and mitotic spindle assembly in C. elegans require SPD-5, a protein with multiple coiled-coil domains. *Dev Cell, 3*(5), 673-684. https://www.ncbi.nlm.nih.gov/pubmed/12431374

Hannak, E., Kirkham, M., Hyman, A. A., & Oegema, K. (2001, Dec 24). Aurora-A kinase is required for centrosome maturation in Caenorhabditis elegans. *J Cell Biol, 155*(7), 1109-1116. https://doi.org/10.1083/jcb.200108051

Hannak, E., Oegema, K., Kirkham, M., Gonczy, P., Habermann, B., & Hyman, A. A. (2002, May 13). The kinetically dominant assembly pathway for centrosomal asters in Caenorhabditis elegans is gamma-tubulin dependent. *J Cell Biol, 157*(4), 591-602. https://doi.org/10.1083/jcb.200202047

Haren, L., Stearns, T., & Luders, J. (2009, Jun 19). Plk1-dependent recruitment of gamma-tubulin complexes to mitotic centrosomes involves multiple PCM components. *PLoS One, 4*(6), e5976. https://doi.org/10.1371/journal.pone.0005976

Hennig, S., Kong, G., Mannen, T., Sadowska, A., Kobelke, S., Blythe, A., Knott, G. J., Iyer, K. S., Ho, D., Newcombe, E. A., Hosoki, K., Goshima, N., Kawaguchi, T., Hatters, D., Trinkle-Mulcahy, L., Hirose, T., Bond, C. S., & Fox, A. H. (2015, Aug 17). Prion-like domains in RNA binding proteins are essential for building subnuclear paraspeckles. *J Cell Biol, 210*(4), 529-539. https://doi.org/10.1083/jcb.201504117

Holehouse, A. S., & Pappu, R. V. (2018, May 1). Functional Implications of Intracellular Phase Transitions. *Biochemistry, 57*(17), 2415-2423. https://doi.org/10.1021/acs.biochem.7b01136

Huang, P. S., Oberdorfer, G., Xu, C., Pei, X. Y., Nannenga, B. L., Rogers, J. M., DiMaio, F., Gonen, T., Luisi, B., & Baker, D. (2014, Oct 24). High thermodynamic stability of parametrically designed helical bundles. *Science, 346*(6208), 481-485. https://doi.org/10.1126/science.1257481

Hutchins, J. R., Toyoda, Y., Hegemann, B., Poser, I., Heriche, J. K., Sykora, M. M., Augsburg, M., Hudecz, O., Buschhorn, B. A., Bulkescher, J., Conrad, C., Comartin, D., Schleiffer, A., Sarov, M., Pozniakovsky, A., Slabicki, M. M., Schloissnig, S., Steinmacher, I., Leuschner, M., Ssykor, A., Lawo, S., Pelletier, L., Stark, H., Nasmyth, K., Ellenberg, J., Durbin, R., Buchholz, F., Mechtler, K., Hyman, A. A., & Peters, J. M. (2010, Apr 30). Systematic analysis of human protein complexes identifies chromosome segregation proteins. *Science, 328*(5978), 593-599. https://doi.org/10.1126/science.1181348

Hyman, A. A., Weber, C. A., & Julicher, F. (2014). Liquid-liquid phase separation in biology. *Annu Rev Cell Dev Biol, 30*, 39-58. https://doi.org/10.1146/annurev-cellbio-100913-013325

886 Jao, L. E., Akef, A., & Wente, S. R. (2017, Jan 01). A role for Gle1, a regulator of DEAD-box
887 RNA helicases, at centrosomes and basal bodies. *Mol Biol Cell, 28*(1), 120-127.
888 https://doi.org/10.1091/mbc.E16-09-0675
889
890 Jeng, R., & Stearns, T. (1999, Sep). Gamma-tubulin complexes: size does matter. *Trends Cell*
891 *Biol, 9*(9), 339-342. https://www.ncbi.nlm.nih.gov/pubmed/10461186
892
893 Jiang, F., Taylor, D. W., Chen, J. S., Kornfeld, J. E., Zhou, K., Thompson, A. J., Nogales, E., &
894 Doudna, J. A. (2016, Feb 19). Structures of a CRISPR-Cas9 R-loop complex primed for
895 DNA cleavage. *Science, 351*(6275), 867-871. https://doi.org/10.1126/science.aad8282
896
897 Jiang, F., Zhou, K., Ma, L., Gressel, S., & Doudna, J. A. (2015, Jun 26). A Cas9-guide RNA
898 complex preorganized for target DNA recognition. *Science, 348*(6242), 1477-1481.
899 https://doi.org/10.1126/science.aab1452
900
901 Jiang, X., Brust-Mascher, I., & Jao, L. E. (2019, Aug 20). Three-dimensional reconstruction and
902 quantification of proteins and mRNAs at the single-cell level in cultured cells. *Bio-protocol,*
903 *9*(16), e3330. https://doi.org/10.21769/BioProtoc.3330
904
905 Joshi, H. C., Palacios, M. J., McNamara, L., & Cleveland, D. W. (1992, Mar 5). Gamma-tubulin
906 is a centrosomal protein required for cell cycle-dependent microtubule nucleation. *Nature,*
907 *356*(6364), 80-83. https://doi.org/10.1038/356080a0
908
909 Joukov, V., Walter, J. C., & De Nicolo, A. (2014, Aug 21). The Cep192-organized aurora A-Plk1
910 cascade is essential for centrosome cycle and bipolar spindle assembly. *Mol Cell, 55*(4),
911 578-591. https://doi.org/10.1016/j.molcel.2014.06.016
912
913 Kalderon, D., Roberts, B. L., Richardson, W. D., & Smith, A. E. (1984, Dec). A short amino acid
914 sequence able to specify nuclear location. *Cell, 39*(3 Pt 2), 499-509.
915 https://doi.org/10.1016/0092-8674(84)90457-4
916
917 Kato, M., Han, T. W., Xie, S., Shi, K., Du, X., Wu, L. C., Mirzaei, H., Goldsmith, E. J., Longgood,
918 J., Pei, J., Grishin, N. V., Frantz, D. E., Schneider, J. W., Chen, S., Li, L., Sawaya, M. R.,
919 Eisenberg, D., Tycko, R., & McKnight, S. L. (2012, May 11). Cell-free formation of RNA
920 granules: low complexity sequence domains form dynamic fibers within hydrogels. *Cell,*
921 *149*(4), 753-767. https://doi.org/10.1016/j.cell.2012.04.017
922
923 Kemp, C. A., Kopish, K. R., Zipperlen, P., Ahringer, J., & O'Connell, K. F. (2004, Apr).
924 Centrosome maturation and duplication in C. elegans require the coiled-coil protein SPD-2.
925 *Dev Cell, 6*(4), 511-523. https://www.ncbi.nlm.nih.gov/pubmed/15068791
926
927 Khodjakov, A., & Rieder, C. L. (1999, Aug 09). The sudden recruitment of gamma-tubulin to the
928 centrosome at the onset of mitosis and its dynamic exchange throughout the cell cycle, do
929 not require microtubules. *J Cell Biol, 146*(3), 585-596.
930 https://www.ncbi.nlm.nih.gov/pubmed/10444067
931
932 Kim, S., & Rhee, K. (2014). Importance of the CEP215-pericentrin interaction for centrosome
933 maturation during mitosis. *PLoS One, 9*(1), e87016.
934 https://doi.org/10.1371/journal.pone.0087016

935
936 Kim, S. I., Oceguera-Yanez, F., Sakurai, C., Nakagawa, M., Yamanaka, S., & Woltjen, K.
937 (2016). Inducible Transgene Expression in Human iPS Cells Using Versatile All-in-One
938 piggyBac Transposons. *Methods Mol Biol, 1357*, 111-131.
939 https://doi.org/10.1007/7651_2015_251
940
941 Kinoshita, K., Noetzel, T. L., Pelletier, L., Mechtler, K., Drechsel, D. N., Schwager, A., Lee, M.,
942 Raff, J. W., & Hyman, A. A. (2005, Sep 26). Aurora A phosphorylation of TACC3/maskin is
943 required for centrosome-dependent microtubule assembly in mitosis. *J Cell Biol, 170*(7),
944 1047-1055. https://doi.org/10.1083/jcb.200503023
945
946 Knop, M., & Schiebel, E. (1997, Dec 1). Spc98p and Spc97p of the yeast gamma-tubulin
947 complex mediate binding to the spindle pole body via their interaction with Spc110p. *EMBO*
948 *J, 16*(23), 6985-6995. https://doi.org/10.1093/emboj/16.23.6985
949
950 Kroschwald, S., Maharana, S., & Simon, A. (2017). Hexanediol: a chemical probe to investigate
951 the material properties of membrane-less compartments. *Matters*.
952 https://doi.org/10.19185/matters.201702000010
953
954 Kwan, K. M., Fujimoto, E., Grabher, C., Mangum, B. D., Hardy, M. E., Campbell, D. S., Parant,
955 J. M., Yost, H. J., Kanki, J. P., & Chien, C. B. (2007, Nov). The Tol2kit: a multisite gateway-
956 based construction kit for Tol2 transposon transgenesis constructs. *Dev Dyn, 236*(11), 3088-
957 3099. https://doi.org/10.1002/dvdy.21343
958
959 Larson, A. G., Elnatan, D., Keenen, M. M., Trnka, M. J., Johnston, J. B., Burlingame, A. L.,
960 Agard, D. A., Redding, S., & Narlikar, G. J. (2017, Jul 13). Liquid droplet formation by
961 HP1alpha suggests a role for phase separation in heterochromatin. *Nature, 547*(7662), 236-
962 240. https://doi.org/10.1038/nature22822
963
964 Lawo, S., Hasegan, M., Gupta, G. D., & Pelletier, L. (2012, Nov). Subdiffraction imaging of
965 centrosomes reveals higher-order organizational features of pericentriolar material. *Nat Cell*
966 *Biol, 14*(11), 1148-1158. https://doi.org/10.1038/ncb2591
967
968 Lee, K., & Rhee, K. (2011, Dec 26). PLK1 phosphorylation of pericentrin initiates centrosome
969 maturation at the onset of mitosis. *J Cell Biol, 195*(7), 1093-1101.
970 https://doi.org/10.1083/jcb.201106093
971
972 Li, Y., Brown, J. H., Reshetnikova, L., Blazsek, A., Farkas, L., Nyitray, L., & Cohen, C. (2003,
973 Jul 17). Visualization of an unstable coiled coil from the scallop myosin rod. *Nature,*
974 *424*(6946), 341-345. https://doi.org/10.1038/nature01801
975
976 Lin, S., Staahl, B. T., Alla, R. K., & Doudna, J. A. (2014, Dec 15). Enhanced homology-directed
977 human genome engineering by controlled timing of CRISPR/Cas9 delivery. *Elife, 3*, e04766.
978 https://doi.org/10.7554/eLife.04766
979
980 Lin, T. C., Neuner, A., Schlosser, Y. T., Scharf, A. N., Weber, L., & Schiebel, E. (2014, Apr 30).
981 Cell-cycle dependent phosphorylation of yeast pericentrin regulates gamma-TuSC-mediated
982 microtubule nucleation. *Elife, 3*, e02208. https://doi.org/10.7554/eLife.02208
983

Lin, Y., Protter, D. S., Rosen, M. K., & Parker, R. (2015, Oct 15). Formation and Maturation of Phase-Separated Liquid Droplets by RNA-Binding Proteins. *Mol Cell, 60*(2), 208-219. https://doi.org/10.1016/j.molcel.2015.08.018

Lindsay, H., Burger, A., Biyong, B., Felker, A., Hess, C., Zaugg, J., Chiavacci, E., Anders, C., Jinek, M., Mosimann, C., & Robinson, M. D. (2016, Jul 12). CrispRVariants charts the mutation spectrum of genome engineering experiments. *Nat Biotechnol, 34*(7), 701-702. https://doi.org/10.1038/nbt.3628

Livingstone, C. D., & Barton, G. J. (1993, Dec). Protein sequence alignments: a strategy for the hierarchical analysis of residue conservation. *Comput Appl Biosci, 9*(6), 745-756. https://doi.org/10.1093/bioinformatics/9.6.745

Lu, Y., Wu, T., Gutman, O., Lu, H., Zhou, Q., Henis, Y. I., & Luo, K. (2020, Mar 23). Phase separation of TAZ compartmentalizes the transcription machinery to promote gene expression. *Nat Cell Biol*. https://doi.org/10.1038/s41556-020-0485-0

Lupas, A., Van Dyke, M., & Stock, J. (1991, May 24). Predicting coiled coils from protein sequences. *Science, 252*(5009), 1162-1164. https://doi.org/10.1126/science.252.5009.1162

Mahen, R., & Venkitaraman, A. R. (2012, Feb). Pattern formation in centrosome assembly. *Curr Opin Cell Biol, 24*(1), 14-23. https://doi.org/10.1016/j.ceb.2011.12.012

Mali, P., Yang, L., Esvelt, K. M., Aach, J., Guell, M., DiCarlo, J. E., Norville, J. E., & Church, G. M. (2013, Feb 15). RNA-guided human genome engineering via Cas9. *Science, 339*(6121), 823-826. https://doi.org/10.1126/science.1232033

Martinez-Campos, M., Basto, R., Baker, J., Kernan, M., & Raff, J. W. (2004, Jun 7). The Drosophila pericentrin-like protein is essential for cilia/flagella function, but appears to be dispensable for mitosis. *J Cell Biol, 165*(5), 673-683. https://doi.org/10.1083/jcb.200402130

Meng, L., Park, J. E., Kim, T. S., Lee, E. H., Park, S. Y., Zhou, M., Bang, J. K., & Lee, K. S. (2015, Aug). Bimodal Interaction of Mammalian Polo-Like Kinase 1 and a Centrosomal Scaffold, Cep192, in the Regulation of Bipolar Spindle Formation. *Mol Cell Biol, 35*(15), 2626-2640. https://doi.org/10.1128/MCB.00068-15

Mennella, V., Agard, D. A., Huang, B., & Pelletier, L. (2014, Mar). Amorphous no more: subdiffraction view of the pericentriolar material architecture. *Trends Cell Biol, 24*(3), 188-197. https://doi.org/10.1016/j.tcb.2013.10.001

Mennella, V., Keszthelyi, B., McDonald, K. L., Chhun, B., Kan, F., Rogers, G. C., Huang, B., & Agard, D. A. (2012, Nov). Subdiffraction-resolution fluorescence microscopy reveals a domain of the centrosome critical for pericentriolar material organization. *Nat Cell Biol, 14*(11), 1159-1168. https://doi.org/10.1038/ncb2597

Merriam, E. B., Millette, M., Lumbard, D. C., Saengsawang, W., Fothergill, T., Hu, X., Ferhat, L., & Dent, E. W. (2013, Oct 16). Synaptic regulation of microtubule dynamics in dendritic spines by calcium, F-actin, and drebrin. *J Neurosci, 33*(42), 16471-16482. https://doi.org/10.1523/JNEUROSCI.0661-13.2013

Mikule, K., Delaval, B., Kaldis, P., Jurcyzk, A., Hergert, P., & Doxsey, S. (2007, Feb). Loss of centrosome integrity induces p38-p53-p21-dependent G1-S arrest. *Nat Cell Biol, 9*(2), 160-170. https://doi.org/10.1038/ncb1529

Molliex, A., Temirov, J., Lee, J., Coughlin, M., Kanagaraj, A. P., Kim, H. J., Mittag, T., & Taylor, J. P. (2015, Sep 24). Phase separation by low complexity domains promotes stress granule assembly and drives pathological fibrillization. *Cell, 163*(1), 123-133. https://doi.org/10.1016/j.cell.2015.09.015

Moritz, M., Braunfeld, M. B., Fung, J. C., Sedat, J. W., Alberts, B. M., & Agard, D. A. (1995, Sep). Three-dimensional structural characterization of centrosomes from early Drosophila embryos. *J Cell Biol, 130*(5), 1149-1159. https://doi.org/10.1083/jcb.130.5.1149

Moritz, M., Braunfeld, M. B., Sedat, J. W., Alberts, B., & Agard, D. A. (1995, Dec 07). Microtubule nucleation by gamma-tubulin-containing rings in the centrosome. *Nature, 378*(6557), 638-640. https://doi.org/10.1038/378638a0

Moritz, M., Zheng, Y., Alberts, B. M., & Oegema, K. (1998, Aug 10). Recruitment of the gamma-tubulin ring complex to Drosophila salt-stripped centrosome scaffolds. *J Cell Biol, 142*(3), 775-786. https://doi.org/10.1083/jcb.142.3.775

Neumann, B., Walter, T., Heriche, J. K., Bulkescher, J., Erfle, H., Conrad, C., Rogers, P., Poser, I., Held, M., Liebel, U., Cetin, C., Sieckmann, F., Pau, G., Kabbe, R., Wunsche, A., Satagopam, V., Schmitz, M. H., Chapuis, C., Gerlich, D. W., Schneider, R., Eils, R., Huber, W., Peters, J. M., Hyman, A. A., Durbin, R., Pepperkok, R., & Ellenberg, J. (2010, Apr 01). Phenotypic profiling of the human genome by time-lapse microscopy reveals cell division genes. *Nature, 464*(7289), 721-727. https://doi.org/10.1038/nature08869

Nott, T. J., Petsalaki, E., Farber, P., Jervis, D., Fussner, E., Plochowietz, A., Craggs, T. D., Bazett-Jones, D. P., Pawson, T., Forman-Kay, J. D., & Baldwin, A. J. (2015, Mar 5). Phase transition of a disordered nuage protein generates environmentally responsive membraneless organelles. *Mol Cell, 57*(5), 936-947. https://doi.org/10.1016/j.molcel.2015.01.013

Numata, S., Iga, J., Nakataki, M., Tayoshi, S., Tanahashi, T., Itakura, M., Ueno, S., & Ohmori, T. (2009, May). Positive association of the pericentrin (PCNT) gene with major depressive disorder in the Japanese population. *J Psychiatry Neurosci, 34*(3), 195-198. https://www.ncbi.nlm.nih.gov/pubmed/19448849

Oakley, B. R., Oakley, C. E., Yoon, Y., & Jung, M. K. (1990, Jun 29). Gamma-tubulin is a component of the spindle pole body that is essential for microtubule function in Aspergillus nidulans. *Cell, 61*(7), 1289-1301. https://doi.org/10.1016/0092-8674(90)90693-9

Oegema, K., Wiese, C., Martin, O. C., Milligan, R. A., Iwamatsu, A., Mitchison, T. J., & Zheng, Y. (1999, Feb 22). Characterization of two related Drosophila gamma-tubulin complexes that differ in their ability to nucleate microtubules. *J Cell Biol, 144*(4), 721-733. https://doi.org/10.1083/jcb.144.4.721

Palazzo, R. E., Vogel, J. M., Schnackenberg, B. J., Hull, D. R., & Wu, X. (2000). Centrosome maturation. *Curr Top Dev Biol, 49*, 449-470. https://www.ncbi.nlm.nih.gov/pubmed/11005031

Patel, A., Lee, H. O., Jawerth, L., Maharana, S., Jahnel, M., Hein, M. Y., Stoynov, S., Mahamid, J., Saha, S., Franzmann, T. M., Pozniakovski, A., Poser, I., Maghelli, N., Royer, L. A., Weigert, M., Myers, E. W., Grill, S., Drechsel, D., Hyman, A. A., & Alberti, S. (2015, Aug 27). A Liquid-to-Solid Phase Transition of the ALS Protein FUS Accelerated by Disease Mutation. *Cell, 162*(5), 1066-1077. https://doi.org/10.1016/j.cell.2015.07.047

Peng, K., Radivojac, P., Vucetic, S., Dunker, A. K., & Obradovic, Z. (2006, Apr 17). Length-dependent prediction of protein intrinsic disorder. *BMC Bioinformatics, 7*, 208. https://doi.org/10.1186/1471-2105-7-208

Peng, K., Vucetic, S., Radivojac, P., Brown, C. J., Dunker, A. K., & Obradovic, Z. (2005, Feb). Optimizing long intrinsic disorder predictors with protein evolutionary information. *J Bioinform Comput Biol, 3*(1), 35-60. https://doi.org/10.1142/s0219720005000886

Piehl, M., Tulu, U. S., Wadsworth, P., & Cassimeris, L. (2004, Feb 10). Centrosome maturation: measurement of microtubule nucleation throughout the cell cycle by using GFP-tagged EB1. *Proc Natl Acad Sci U S A, 101*(6), 1584-1588. https://doi.org/10.1073/pnas.0308205100

Raff, J. W. (2019, May 7). Phase Separation and the Centrosome: A Fait Accompli? *Trends Cell Biol*. https://doi.org/10.1016/j.tcb.2019.04.001

Rauch, A., Thiel, C. T., Schindler, D., Wick, U., Crow, Y. J., Ekici, A. B., van Essen, A. J., Goecke, T. O., Al-Gazali, L., Chrzanowska, K. H., Zweier, C., Brunner, H. G., Becker, K., Curry, C. J., Dallapiccola, B., Devriendt, K., Dorfler, A., Kinning, E., Megarbane, A., Meinecke, P., Semple, R. K., Spranger, S., Toutain, A., Trembath, R. C., Voss, E., Wilson, L., Hennekam, R., de Zegher, F., Dorr, H. G., & Reis, A. (2008, Feb 8). Mutations in the pericentrin (PCNT) gene cause primordial dwarfism. *Science, 319*(5864), 816-819. https://doi.org/10.1126/science.1151174

Riback, J. A., Katanski, C. D., Kear-Scott, J. L., Pilipenko, E. V., Rojek, A. E., Sosnick, T. R., & Drummond, D. A. (2017, Mar 9). Stress-Triggered Phase Separation Is an Adaptive, Evolutionarily Tuned Response. *Cell, 168*(6), 1028-1040 e1019. https://doi.org/10.1016/j.cell.2017.02.027

Ribbeck, K., & Gorlich, D. (2002, Jun 3). The permeability barrier of nuclear pore complexes appears to operate via hydrophobic exclusion. *EMBO J, 21*(11), 2664-2671. https://doi.org/10.1093/emboj/21.11.2664

Rieder, C. L., & Borisy, G. G. (1982). The centrosome cycle in PtK2 cells: Asymmetric distribution and structural changes in the pericentriolar material. *Biology of the Cell, 44*, 117-132.

Romero, P., Obradovic, Z., & Dunker, A. K. (1999, Dec 3). Folding minimal sequences: the lower bound for sequence complexity of globular proteins. *FEBS Lett, 462*(3), 363-367. https://doi.org/10.1016/s0014-5793(99)01557-4

Rose, A., & Meier, I. (2004, Aug). Scaffolds, levers, rods and springs: diverse cellular functions of long coiled-coil proteins. *Cell Mol Life Sci, 61*(16), 1996-2009. https://doi.org/10.1007/s00018-004-4039-6

Salisbury, J. L. (2003, Feb 4). Centrosomes: coiled-coils organize the cell center. *Curr Biol, 13*(3), R88-90. https://doi.org/10.1016/s0960-9822(03)00033-2

Sanders, A., Chang, K., Zhu, X., Thoppil, R. J., Holmes, W. R., & Kaverina, I. (2017, Nov 7). Nonrandom gamma-TuNA-dependent spatial pattern of microtubule nucleation at the Golgi. *Mol Biol Cell, 28*(23), 3181-3192. https://doi.org/10.1091/mbc.E17-06-0425

Schnackenberg, B. J., Khodjakov, A., Rieder, C. L., & Palazzo, R. E. (1998, Aug 4). The disassembly and reassembly of functional centrosomes in vitro. *Proc Natl Acad Sci U S A, 95*(16), 9295-9300. https://doi.org/10.1073/pnas.95.16.9295

Schnackenberg, B. J., & Palazzo, R. E. (1999, Jul). Identification and function of the centrosome centromatrix. *Biol Cell, 91*(6), 429-438. https://www.ncbi.nlm.nih.gov/pubmed/10576861

Sepulveda, G., Antkowiak, M., Brust-Mascher, I., Mahe, K., Ou, T., Castro, N. M., Christensen, L. N., Cheung, L., Jiang, X., Yoon, D., Huang, B., & Jao, L. E. (2018, Apr 30). Co-translational protein targeting facilitates centrosomal recruitment of PCNT during centrosome maturation in vertebrates. *Elife, 7*, pii: e34959. doi: 34910.37554/eLife.34959. https://doi.org/10.7554/eLife.34959

Shcherbakova, D. M., Baloban, M., Emelyanov, A. V., Brenowitz, M., Guo, P., & Verkhusha, V. V. (2016, Aug 19). Bright monomeric near-infrared fluorescent proteins as tags and biosensors for multiscale imaging. *Nat Commun, 7*, 12405. https://doi.org/10.1038/ncomms12405

Shin, Y., & Brangwynne, C. P. (2017, Sep 22). Liquid phase condensation in cell physiology and disease. *Science, 357*(6357). https://doi.org/10.1126/science.aaf4382

Smith, J., Calidas, D., Schmidt, H., Lu, T., Rasoloson, D., & Seydoux, G. (2016, Dec 3). Spatial patterning of P granules by RNA-induced phase separation of the intrinsically-disordered protein MEG-3. *Elife, 5*. https://doi.org/10.7554/eLife.21337

So, C., Seres, K. B., Steyer, A. M., Monnich, E., Clift, D., Pejkovska, A., Mobius, W., & Schuh, M. (2019, Jun 28). A liquid-like spindle domain promotes acentrosomal spindle assembly in mammalian oocytes. *Science, 364*(6447). https://doi.org/10.1126/science.aat9557

Sonnen, K. F., Schermelleh, L., Leonhardt, H., & Nigg, E. A. (2012, Oct 15). 3D-structured illumination microscopy provides novel insight into architecture of human centrosomes. *Biol Open, 1*(10), 965-976. https://doi.org/10.1242/bio.20122337

Sonnichsen, B., Koski, L. B., Walsh, A., Marschall, P., Neumann, B., Brehm, M., Alleaume, A. M., Artelt, J., Bettencourt, P., Cassin, E., Hewitson, M., Holz, C., Khan, M., Lazik, S., Martin, C., Nitzsche, B., Ruer, M., Stamford, J., Winzi, M., Heinkel, R., Roder, M., Finell, J., Hantsch, H., Jones, S. J., Jones, M., Piano, F., Gunsalus, K. C., Oegema, K., Gonczy, P.,

Coulson, A., Hyman, A. A., & Echeverri, C. J. (2005, Mar 24). Full-genome RNAi profiling of early embryogenesis in Caenorhabditis elegans. *Nature, 434*(7032), 462-469. https://doi.org/10.1038/nature03353

Stearns, T., Evans, L., & Kirschner, M. (1991, May 31). Gamma-tubulin is a highly conserved component of the centrosome. *Cell, 65*(5), 825-836. https://doi.org/10.1016/0092-8674(91)90390-k

Stearns, T., & Kirschner, M. (1994, Feb 25). In vitro reconstitution of centrosome assembly and function: the central role of gamma-tubulin. *Cell, 76*(4), 623-637. https://doi.org/10.1016/0092-8674(94)90503-7

Strom, A. R., Emelyanov, A. V., Mir, M., Fyodorov, D. V., Darzacq, X., & Karpen, G. H. (2017, Jul 13). Phase separation drives heterochromatin domain formation. *Nature, 547*(7662), 241-245. https://doi.org/10.1038/nature22989

Sundberg, H. A., & Davis, T. N. (1997, Dec). A mutational analysis identifies three functional regions of the spindle pole component Spc110p in Saccharomyces cerevisiae. *Mol Biol Cell, 8*(12), 2575-2590. https://doi.org/10.1091/mbc.8.12.2575

Szappanos, B., Suveges, D., Nyitray, L., Perczel, A., & Gaspari, Z. (2010, Apr 16). Folded-unfolded cross-predictions and protein evolution: the case study of coiled-coils. *FEBS Lett, 584*(8), 1623-1627. https://doi.org/10.1016/j.febslet.2010.03.026

Takahashi, M., Yamagiwa, A., Nishimura, T., Mukai, H., & Ono, Y. (2002, Sep). Centrosomal proteins CG-NAP and kendrin provide microtubule nucleation sites by anchoring gamma-tubulin ring complex. *Mol Biol Cell, 13*(9), 3235-3245. https://doi.org/10.1091/mbc.e02-02-0112

Thomson, A. R., Wood, C. W., Burton, A. J., Bartlett, G. J., Sessions, R. B., Brady, R. L., & Woolfson, D. N. (2014, Oct 24). Computational design of water-soluble alpha-helical barrels. *Science, 346*(6208), 485-488. https://doi.org/10.1126/science.1257452

Tynan, S. H., Purohit, A., Doxsey, S. J., & Vallee, R. B. (2000, Oct 20). Light intermediate chain 1 defines a functional subfraction of cytoplasmic dynein which binds to pericentrin. *J Biol Chem, 275*(42), 32763-32768. https://doi.org/10.1074/jbc.M001536200

Uversky, V. N., Gillespie, J. R., & Fink, A. L. (2000, Nov 15). Why are "natively unfolded" proteins unstructured under physiologic conditions? *Proteins, 41*(3), 415-427. https://doi.org/10.1002/1097-0134(20001115)41:3<415::aid-prot130>3.0.co;2-7

Vega, I. E., Umstead, A., & Kanaan, N. M. (2019). EFhd2 Affects Tau Liquid-Liquid Phase Separation. *Front Neurosci, 13*, 845. https://doi.org/10.3389/fnins.2019.00845

Vorobjev, I. A., & Chentsov Yu, S. (1982, Jun). Centrioles in the cell cycle. I. Epithelial cells. *J Cell Biol, 93*(3), 938-949. https://doi.org/10.1083/jcb.93.3.938

Wang, J., Choi, J. M., Holehouse, A. S., Lee, H. O., Zhang, X., Jahnel, M., Maharana, S., Lemaitre, R., Pozniakovsky, A., Drechsel, D., Poser, I., Pappu, R. V., Alberti, S., & Hyman,

A. A. (2018, Jul 26). A Molecular Grammar Governing the Driving Forces for Phase Separation of Prion-like RNA Binding Proteins. *Cell, 174*(3), 688-699 e616. https://doi.org/10.1016/j.cell.2018.06.006

Wang, W. J., Soni, R. K., Uryu, K., & Tsou, M. F. (2011, May 16). The conversion of centrioles to centrosomes: essential coupling of duplication with segregation. *J Cell Biol, 193*(4), 727-739. https://doi.org/10.1083/jcb.201101109

Waterhouse, A. M., Procter, J. B., Martin, D. M., Clamp, M., & Barton, G. J. (2009, May 1). Jalview Version 2--a multiple sequence alignment editor and analysis workbench. *Bioinformatics, 25*(9), 1189-1191. https://doi.org/10.1093/bioinformatics/btp033

Wegmann, S., Eftekharzadeh, B., Tepper, K., Zoltowska, K. M., Bennett, R. E., Dujardin, S., Laskowski, P. R., MacKenzie, D., Kamath, T., Commins, C., Vanderburg, C., Roe, A. D., Fan, Z., Molliex, A. M., Hernandez-Vega, A., Muller, D., Hyman, A. A., Mandelkow, E., Taylor, J. P., & Hyman, B. T. (2018, Apr 3). Tau protein liquid-liquid phase separation can initiate tau aggregation. *EMBO J, 37*(7). https://doi.org/10.15252/embj.201798049

Wippich, F., Bodenmiller, B., Trajkovska, M. G., Wanka, S., Aebersold, R., & Pelkmans, L. (2013, Feb 14). Dual specificity kinase DYRK3 couples stress granule condensation/dissolution to mTORC1 signaling. *Cell, 152*(4), 791-805. https://doi.org/10.1016/j.cell.2013.01.033

Woodruff, J. B., Ferreira Gomes, B., Widlund, P. O., Mahamid, J., Honigmann, A., & Hyman, A. A. (2017, Jun 1). The Centrosome Is a Selective Condensate that Nucleates Microtubules by Concentrating Tubulin. *Cell, 169*(6), 1066-1077 e1010. https://doi.org/10.1016/j.cell.2017.05.028

Woodruff, J. B., Wueseke, O., & Hyman, A. A. (2014, Sep 05). Pericentriolar material structure and dynamics. *Philos Trans R Soc Lond B Biol Sci, 369*(1650). https://doi.org/10.1098/rstb.2013.0459

Woodruff, J. B., Wueseke, O., Viscardi, V., Mahamid, J., Ochoa, S. D., Bunkenborg, J., Widlund, P. O., Pozniakovsky, A., Zanin, E., Bahmanyar, S., Zinke, A., Hong, S. H., Decker, M., Baumeister, W., Andersen, J. S., Oegema, K., & Hyman, A. A. (2015, May 15). Regulated assembly of a supramolecular centrosome scaffold in vitro. *Science, 348*(6236), 808-812. https://doi.org/10.1126/science.aaa3923

Wootton, J. C. (1994, Sep). Non-globular domains in protein sequences: automated segmentation using complexity measures. *Comput Chem, 18*(3), 269-285. https://www.ncbi.nlm.nih.gov/pubmed/7952898

Wueseke, O., Zwicker, D., Schwager, A., Wong, Y. L., Oegema, K., Julicher, F., Hyman, A. A., & Woodruff, J. B. (2016, Oct 15). Polo-like kinase phosphorylation determines Caenorhabditis elegans centrosome size and density by biasing SPD-5 toward an assembly-competent conformation. *Biol Open, 5*(10), 1431-1440. https://doi.org/10.1242/bio.020990

1277 Zeng, M., Shang, Y., Araki, Y., Guo, T., Huganir, R. L., & Zhang, M. (2016, Aug 25). Phase
1278 Transition in Postsynaptic Densities Underlies Formation of Synaptic Complexes and
1279 Synaptic Plasticity. *Cell, 166*(5), 1163-1175 e1112. https://doi.org/10.1016/j.cell.2016.07.008
1280
1281 Zhang, J. P., Li, X. L., Li, G. H., Chen, W., Arakaki, C., Botimer, G. D., Baylink, D., Zhang, L.,
1282 Wen, W., Fu, Y. W., Xu, J., Chun, N., Yuan, W., Cheng, T., & Zhang, X. B. (2017, Feb 20).
1283 Efficient precise knockin with a double cut HDR donor after CRISPR/Cas9-mediated double-
1284 stranded DNA cleavage. *Genome Biol, 18*(1), 35. https://doi.org/10.1186/s13059-017-1164-
1285 8
1286
1287 Zhang, Q., Huang, H., Zhang, L., Wu, R., Chung, C. I., Zhang, S. Q., Torra, J., Schepis, A.,
1288 Coughlin, S. R., Kornberg, T. B., & Shu, X. (2018, Jan 18). Visualizing Dynamics of Cell
1289 Signaling In Vivo with a Phase Separation-Based Kinase Reporter. *Mol Cell, 69*(2), 347.
1290 https://doi.org/10.1016/j.molcel.2018.01.008
1291
1292 Zheng, Y., Jung, M. K., & Oakley, B. R. (1991, May 31). Gamma-tubulin is present in Drosophila
1293 melanogaster and Homo sapiens and is associated with the centrosome. *Cell, 65*(5), 817-
1294 823. https://doi.org/10.1016/0092-8674(91)90389-g
1295
1296 Zheng, Y., Wong, M. L., Alberts, B., & Mitchison, T. (1995, Dec 07). Nucleation of microtubule
1297 assembly by a gamma-tubulin-containing ring complex. *Nature, 378*(6557), 578-583.
1298 https://doi.org/10.1038/378578a0
1299
1300 Zimmerman, W. C., Sillibourne, J., Rosa, J., & Doxsey, S. J. (2004, Aug). Mitosis-specific
1301 anchoring of gamma tubulin complexes by pericentrin controls spindle organization and
1302 mitotic entry. *Mol Biol Cell, 15*(8), 3642-3657. https://doi.org/10.1091/mbc.E03-11-0796
1303
1304 Zwicker, D., Decker, M., Jaensch, S., Hyman, A. A., & Julicher, F. (2014, Jul 1). Centrosomes
1305 are autocatalytic droplets of pericentriolar material organized by centrioles. *Proc Natl Acad
1306 Sci U S A, 111*(26), E2636-2645. https://doi.org/10.1073/pnas.1404855111

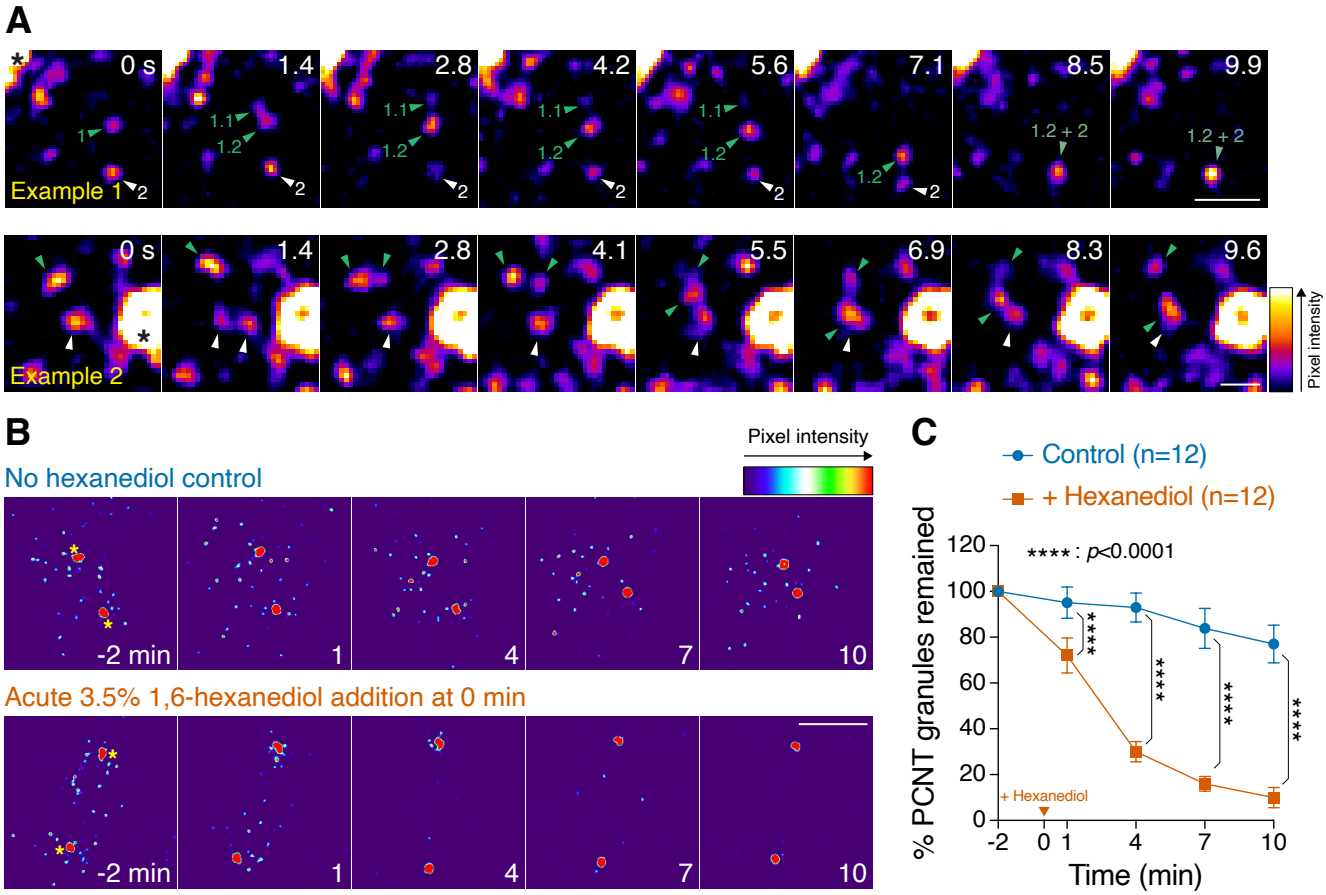

Figure 1. Endogenously expressed GFP-PCNT forms liquid-like condensates during early mitosis. (**A**) Time-lapse micrographs of GFP-PCNT expressed from its endogenous locus during early mitosis. Arrowheads denote the fusing and splitting events of the GFP-PCNT granules. Asterisks in time 0 s denote the centrosomes. The experiment was repeated three times with similar results. (**B**) Time-lapse micrographs of early mitotic cells showing pericentrosomal GFP-PCNT granules without or with the acute 3.5% 1,6-hexanediol treatment. Time 0 is set at the time of hexanediol addition. Asterisks in time -2 min denote the centrosomes. (**C**) Quantification of the results from the experiments shown in (B). Percent of GFP-PCNT granules remained, without and with the acute 1,6-hexanediol treatment, as the function of time was plotted and represented as mean ± 95% CI (confidence intervals) from three biological replicates. The total number of cells analyzed for each condition is indicated. The arrowhead denotes the time of hexanediol addition (time 0). p-values were determined by two-tailed Student's t-test. Scale bars, 1 μm (A, Example 1), 0.5 μm (A, Example 2), and 5 μm (B).

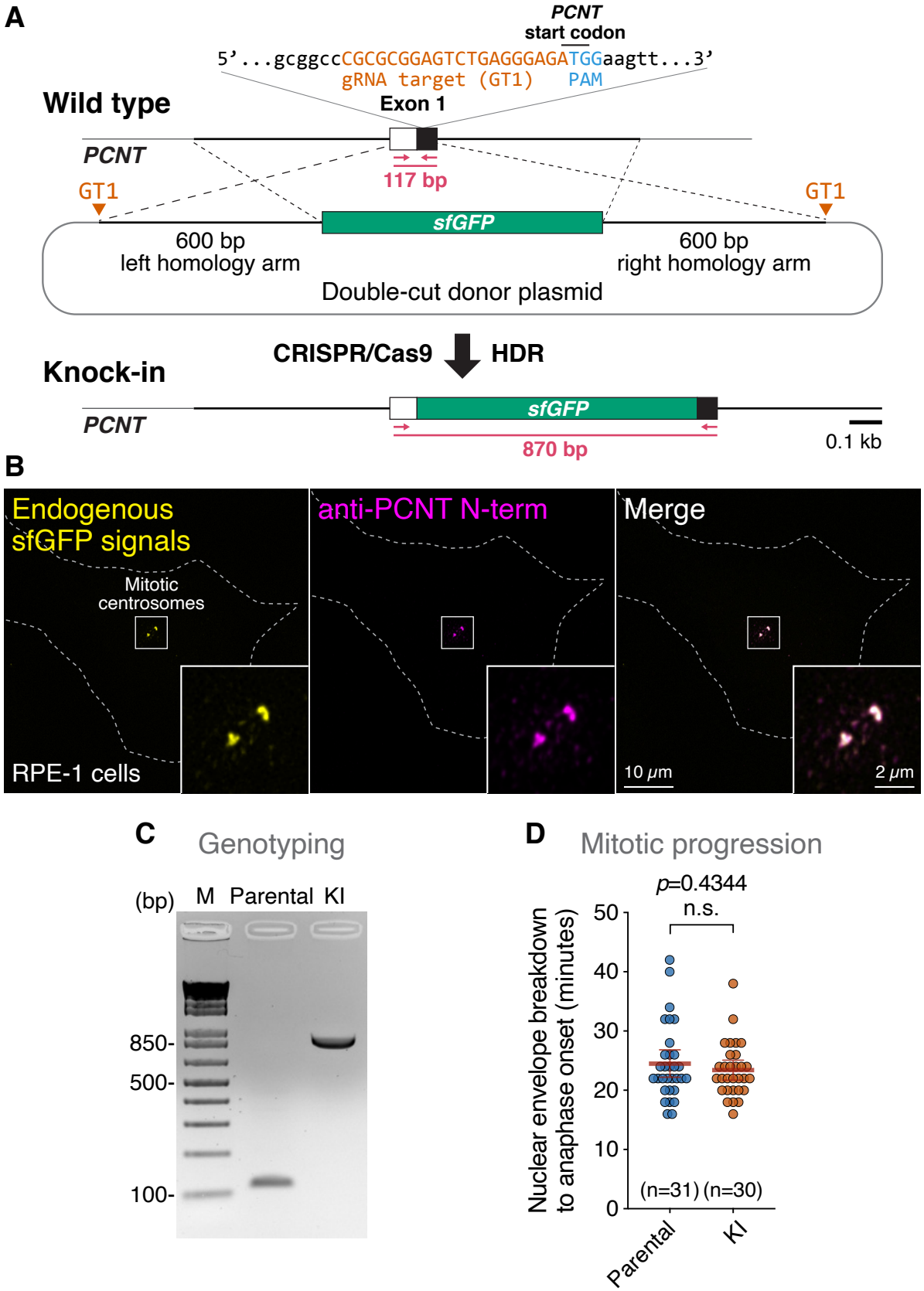

Figure 1- figure supplement 1. Generation and validation of GFP-PCNT knock-in cells. (**A**) Schematic of knocking in *sfGFP* into the *PCNT* locus of RPE-1 cells using the CRISPR/Cas9 technology with a double-cut homology-directed repair (HDR) donor. Arrows indicate the locations of genotyping primers. (**B**) Immunofluorescence images of GFP-PCNT knock-in (KI) cells. The experiment was repeated three times with similar results. (**C**) Genotyping results of the GFP-PCNT KI and the parental cells by polymerase chain reaction (PCR) using the primers indicated in (A). The experiment was repeated three times with similar results. (**D**) Quantification of mitotic durations of GFP-PCNT KI and parental cells stably expressing miRFP670-CETN2 and mScarlet-i-H2A that mark the centrosome and DNA, respectively. Data are mean ± 95% CI. The p-value was determined by two-tailed Student's t-test; n.s., not significant. n, number of cells analyzed from three biological replicates.

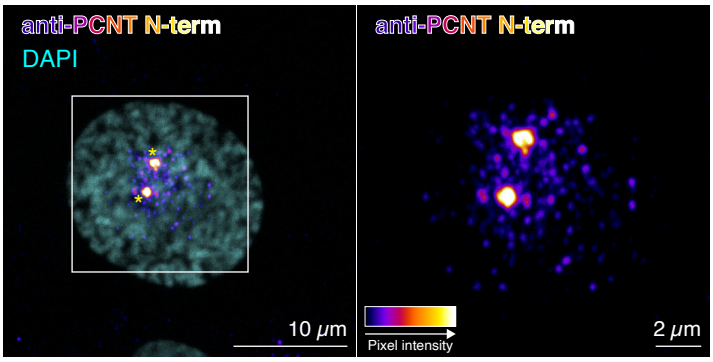

Figure 1- figure supplement 2. PCNT granules near centrosomes during early mitosis. Immunofluorescence of a prophase RPE-1 cell using the anti-PCNT N-terminus antibody to detect endogenous PCNT proteins. Asterisks denote the centrosomes. The experiment was repeated three times with similar results.

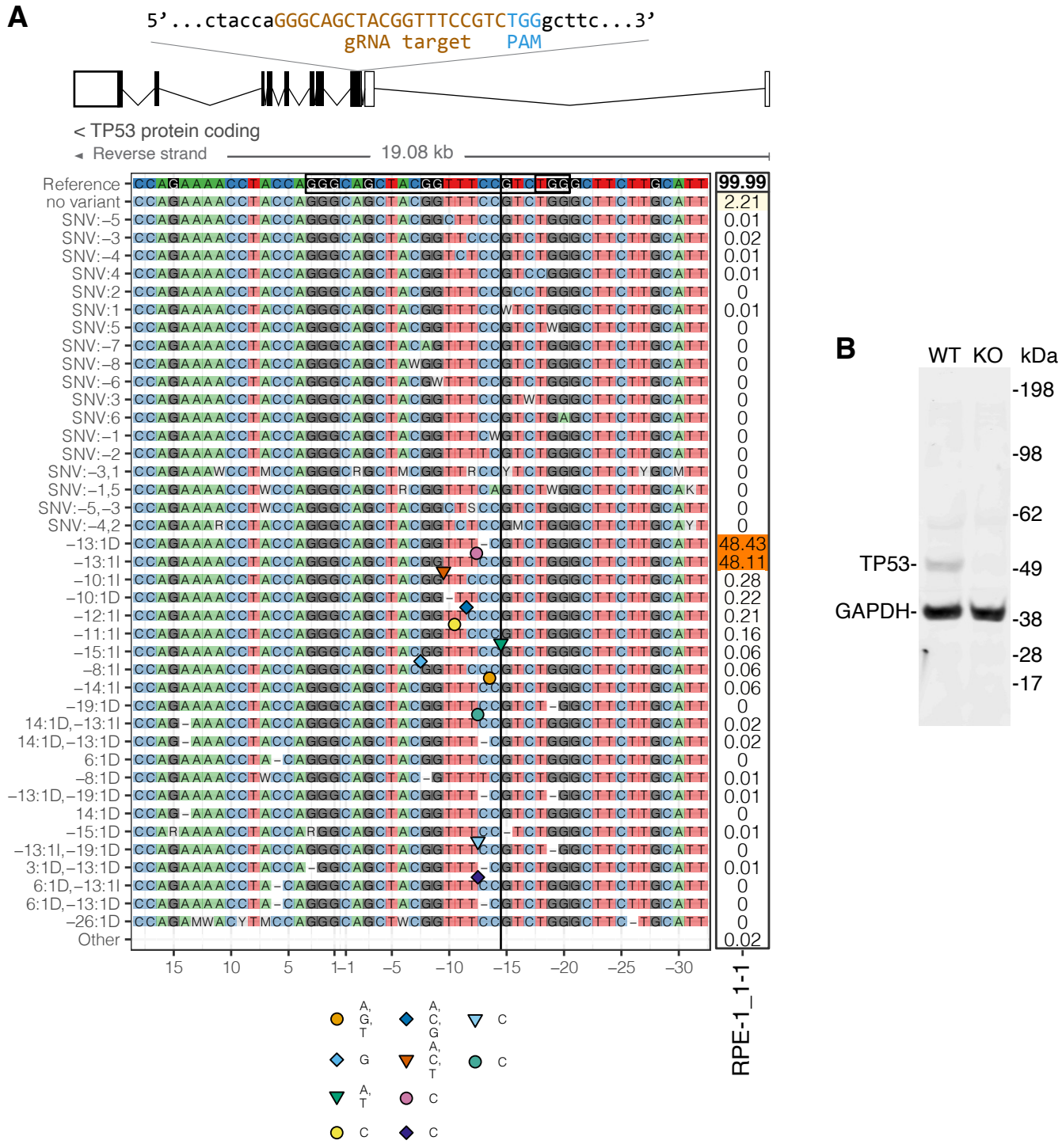

Figure 1- figure supplement 3. Generation of *TP53* knockout RPE-1 cells. (**A**) Illumina sequencing confirmed that one of the CRISPR-edited RPE-1 cell lines, RPE-1_1-1, has frameshift mutations at the gRNA target site in both *TP53* alleles (a 1-bp deletion and a 1-bp insertion). Sequencing data were analyzed and illustrated by an R-based toolkit, CrispRVariants (Lindsay et al., 2016). (**B**) Western blot analysis confirmed the loss of TP53 protein in RPE-1_1-1 cells. Anti-GAPDH staining served as the loading control. WT: parental RPE-1 cells; KO: RPE-1_1-1 cells.

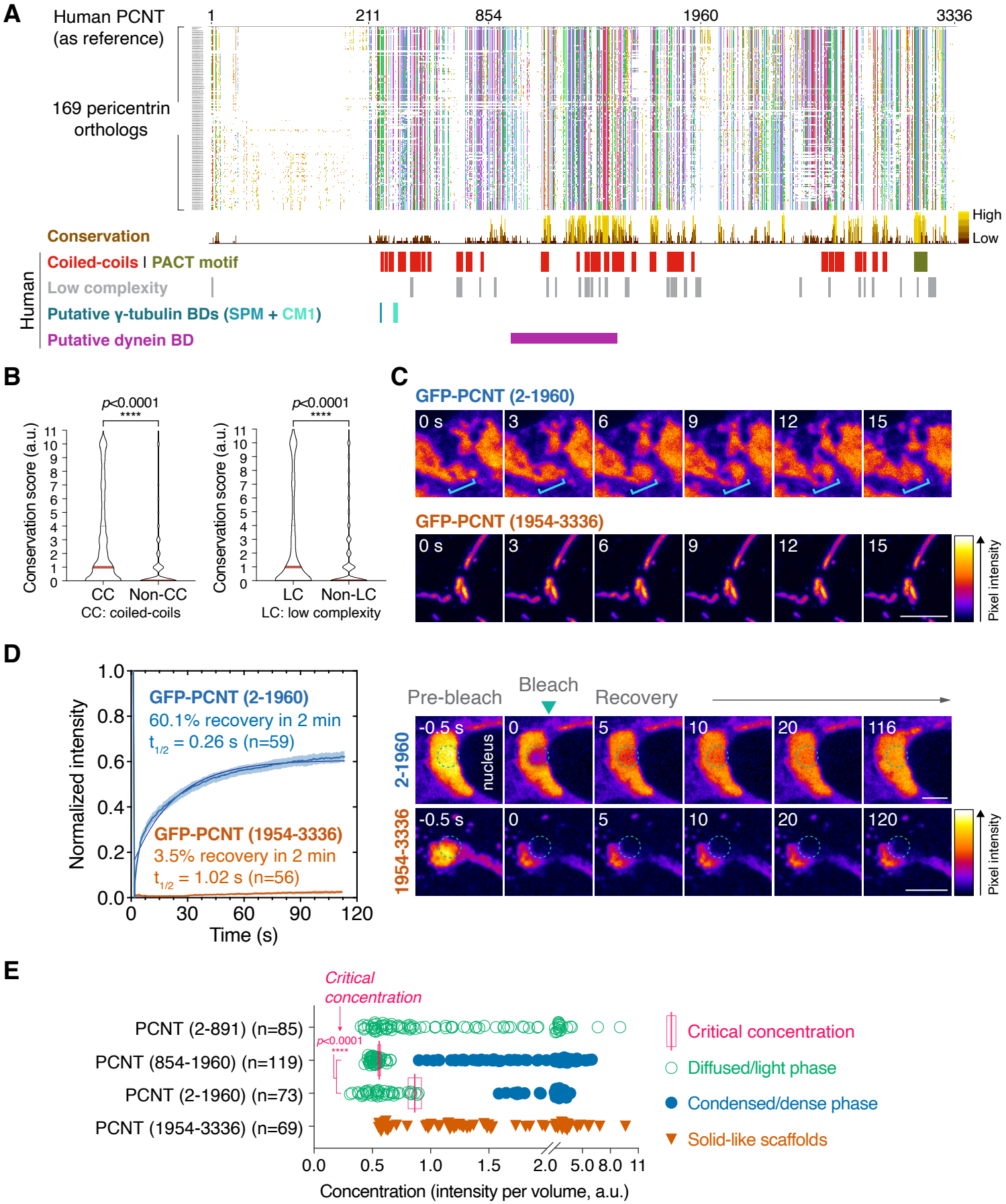
A
Human PCNT (as reference)
1
211
854
1960
3336
169 pericentrin orthologs
High
Low
Conservation
Human
Coiled-coils | PACT motif
Low complexity
Putative γ-tubulin BDs (SPM + CM1)
Putative dynein BD
B
p<0.0001
****
Conservation score (a.u.)
CC
Non-CC
CC: coiled-coils
LC
Non-LC
LC: low complexity
C
GFP-PCNT (2-1960)
GFP-PCNT (1954-3336)
0 s
3
6
9
12
15
Pixel intensity
D
Normalized intensity
GFP-PCNT (2-1960)
60.1% recovery in 2 min
t1/2 = 0.26 s (n=59)
GFP-PCNT (1954-3336)
3.5% recovery in 2 min
t1/2 = 1.02 s (n=56)
Time (s)
Pre-bleach
Bleach
Recovery
2-1960
1954-3336
-0.5 s
nucleus
0
5
10
20
116
120
E
Critical concentration
PCNT (2-891) (n=85)
PCNT (854-1960) (n=119)
PCNT (2-1960) (n=73)
PCNT (1954-3336) (n=69)
p<0.0001
****
Concentration (intensity per volume, a.u.)
Critical concentration
Diffused/light phase
Condensed/dense phase
Solid-like scaffolds

Figure 2. Coiled-coil/LCR-rich N-terminal and middle segments of PCNT phase separate in a concentration-dependent manner. (**A**) An alignment of 169 pericentrin orthologous proteins from vertebrates (167), fruit fly (1), and budding yeast (1) with the conservation scores shown below the alignment. The alignment was colored by the default Clustal X coloring scheme (Figure 2- table 1). Locations of predicted coiled-coils, PACT motif, low-complexity regions, and putative γ-tubulin and dynein binding domains (BDs) of human PCNT are noted below the alignment. (**B**) Distribution of conservation scores corresponding to human PCNT within or outside of the coiled-coil (CC) or low complexity (LC) regions. Data are presented in violin plots, with red bars and dashed lines denoting the median and third quartile, respectively. (**C**) Representative time-lapse micrographs of GFP-tagged PCNT (2-1960) and PCNT (854-1960) 24 h post Dox induction in RPE-1 cells. Brackets denote the dynamic rearrangement of GFP-PCNT (2-1960) condensates. Similar results were observed in three biological replicates. (**D**) FRAP analyses of GFP-PCNT (2-1960) condensates and GFP-PCNT (1954-3336) scaffolds in RPE-1 cells. Dashed circles delineate the bleached sites. Data are mean ± 95% CI. n, number of condensates/scaffolds analyzed from >3 biological replicates. The percent recovery and half-life ($t_{1/2}$) after photobleaching were calculated after fitting the data with non-linear regression. (**E**) Quantification of relative protein concentrations (intensity sum per volume) in live cells expressing various GFP-tagged PCNT segments after Dox induction. Critical concentrations are mean ± 95% CI. n, number of cells analyzed from three biological replicates per segment. The p-values were determined by two-tailed Student's t-test. a.u., arbitrary unit. Scale bars, 5 μm.

Category	Color	Residue at position	{Threshold, Residue group}
Hydrophobic	BLUE	A, I, L, M, F, W, V	{>60%, WLVIMAFCHP}
		C	{>60%, WLVIMAFCHP}
Positive charge	RED	K, R	{>60%, KR}, {>80%, K, R, Q}
Negative charge	MAGENTA	E	{>60%, KR}, {>50%, QE}, {>85%, E, Q, D}
		D	{>60%, KR}, {>85%, K, R, Q}, {>50%, ED}
Polar	GREEN	N	{>50%, N}, {>85%, N,Y}
		Q	{>60%, KR}, {>50%, QE}, {>85%, Q, E, K, R}
		S, T	{>60%, WLVIMAFCHP}, {>50%, TS}, {>85%, S, T}
Cysteines	PINK	C	{>85%, C}
Glycines	ORANGE	G	{>0%, G}
Prolines	YELLOW	P	{>0%, P}
Aromatic	CYAN	H, Y	{>60%, WLVIMAFCHP}, {>85%, W, Y, A, C, P, Q, F, H, I, L, M, V}
Unconserved	WHITE	any/gap	If none of the above criteria are met

Figure 2- table 1. Clustal X coloring scheme (adapted from Jalview) used in the multi-species alignment in Figure 2A.

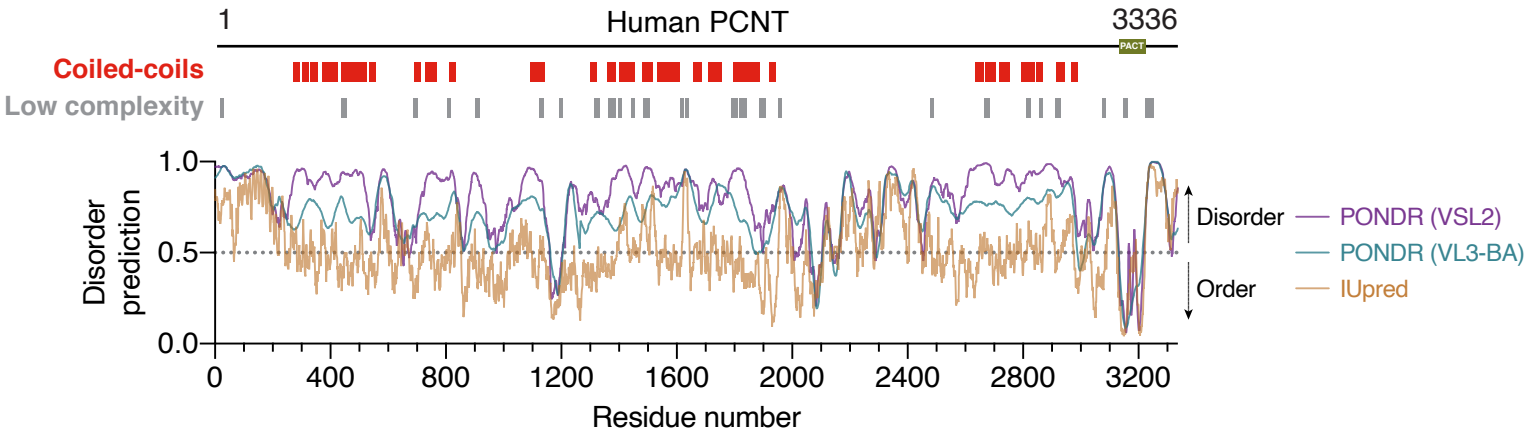

Figure 2- figure supplement 1. Disorder predictions of human PCNT. Predicted coiled-coils and low-complexity regions of human PCNT aligned with results of three disorder prediction algorithms (PONDR VSL2, PONDR VL3-BA, and IUpred).

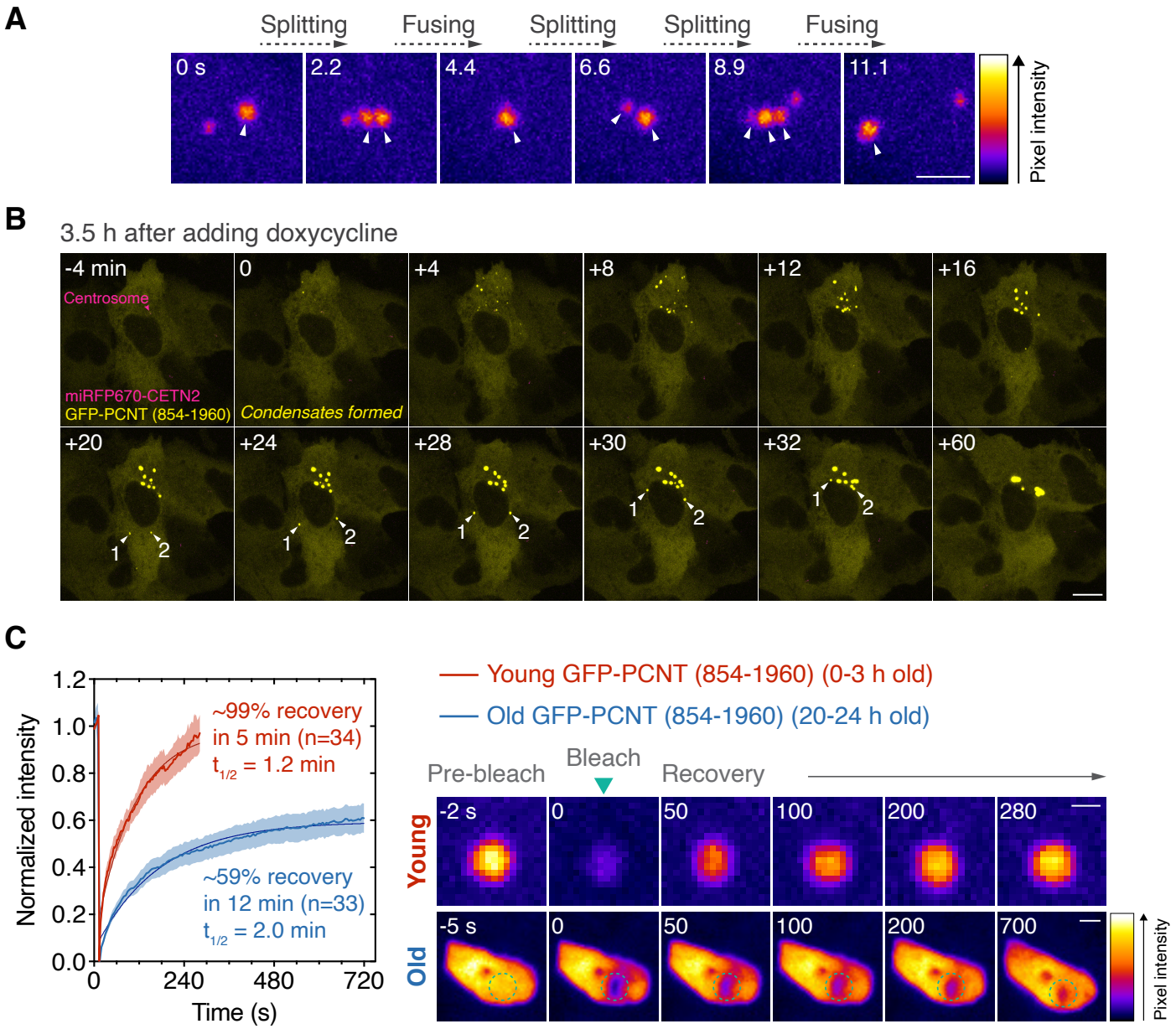

Figure 3. GFP-PCNT (854-1960) undergoes liquid-liquid phase separation, coalesces, and moves toward the centrosome. (**A**) Time-lapse micrographs of GFP-PCNT (854-1960) condensates in RPE-1 cells. Arrowheads denote the fast fusing and splitting events of the spherical condensates. Similar results were observed in three biological replicates. (**B**) Time-lapse micrographs of GFP-PCNT (854-1960) expressed in miRFP670-CETN2-positive RPE-1 cells. Time-lapse imaging started 3.5 h post Dox induction. The time when the first condensates formed is marked as time 0. Arrowheads denote the examples of two condensates moving around the nucleus toward the centrosome. The experiment was repeated more than three times with similar results. (**C**) FRAP analysis of different ages of GFP-PCNT (854-1960) condensates in RPE-1 cells. Dashed circles delineate the bleached sites. Data are mean ± CI. n, number of condensates analyzed from three biological replicates. The percent recovery and half-life ($t_{1/2}$) after photobleaching were calculated after fitting the data with non-linear regression. Note that the highly mobile nature of young condensates prevented us from tracking the same condensates consistently beyond 5 min in the recovery phase of the FRAP assay. Scale bars, 2 μm (A), 10 μm (B), 1 μm (C, young condensates), and 2 μm (C, old condensates).

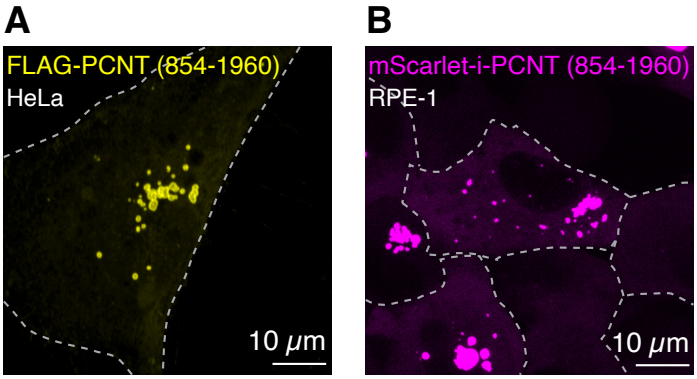

Figure 3- figure supplement 1. FLAG- and mScarlet-i-tagged PCNT (854-1960) fusion proteins form condensates. (**A**) Anti-PCNT N-terminus immunofluorescence of HeLa cells transiently expressing FLAG-PCNT (854-1960). The experiment was repeated two times with similar results. (**B**) mScarlet-i-PCNT (854-1960) condensates in live RPE-1 cells. Dashed lines delineate the cell boundaries. The experiment was repeated three times with similar results.

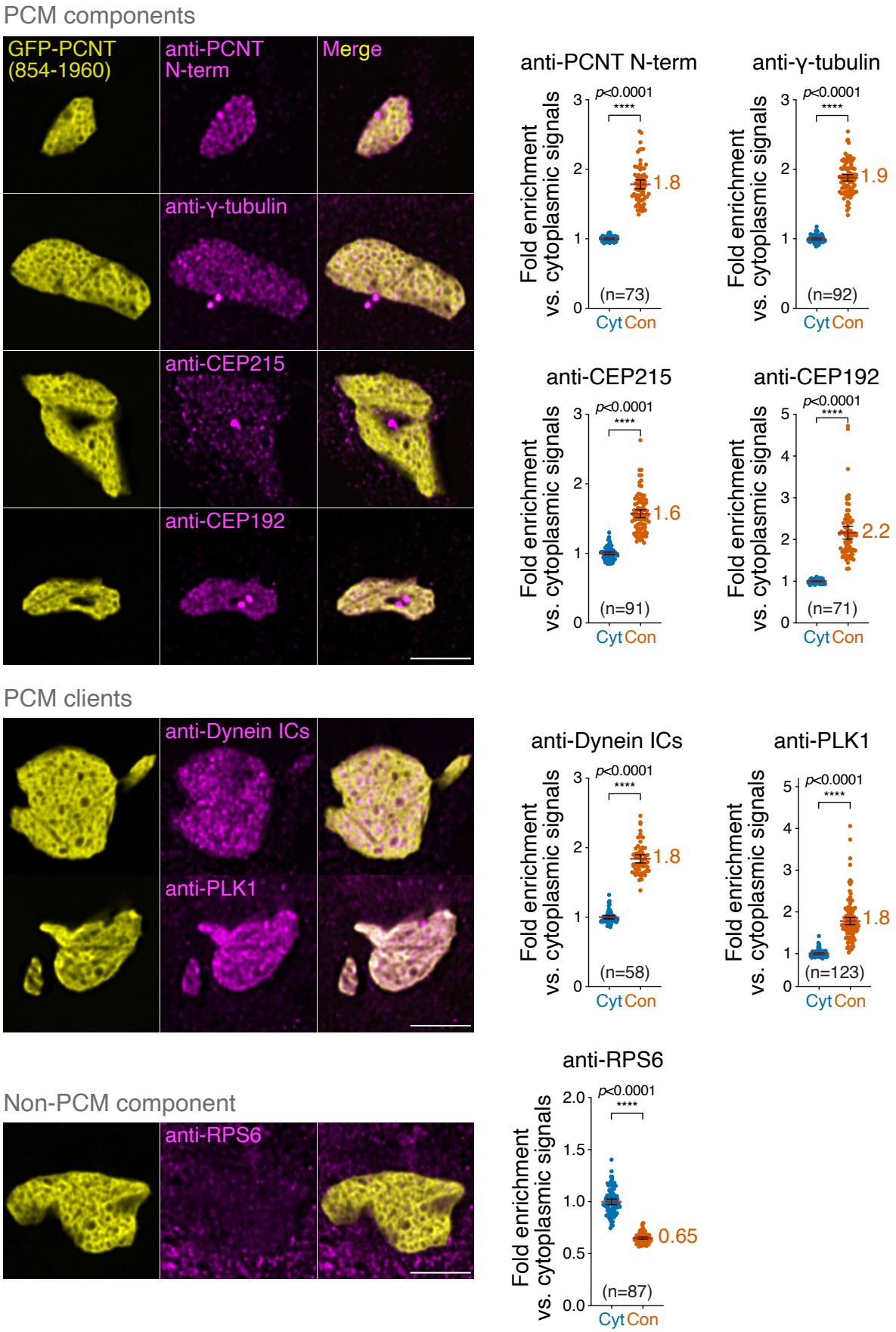

Figure 4. GFP-PCNT (854-1960) condensates selectively recruit endogenous PCM components. Immunofluorescence of PCNT N-terminus (PCNT N-term), γ-tubulin, CEP215, CEP192, cytoplasmic dynein intermediate chains (Dynein ICs), PLK1, or ribosomal protein S6 (RPS6) in RPE-1 cells after Dox induction to form GFP-PCNT (854-1960) condensates. Fold enrichment of fluorescence signals in the condensate (Con) relative to those in the cytoplasm (Cyt) was quantified. Data are mean ± 95% CI. Fold enrichment mean values are noted. n, number of cells analyzed from at least two biological replicates per protein. p-values were determined by two-tailed Student's t-test. Scale bars, 5 μm.

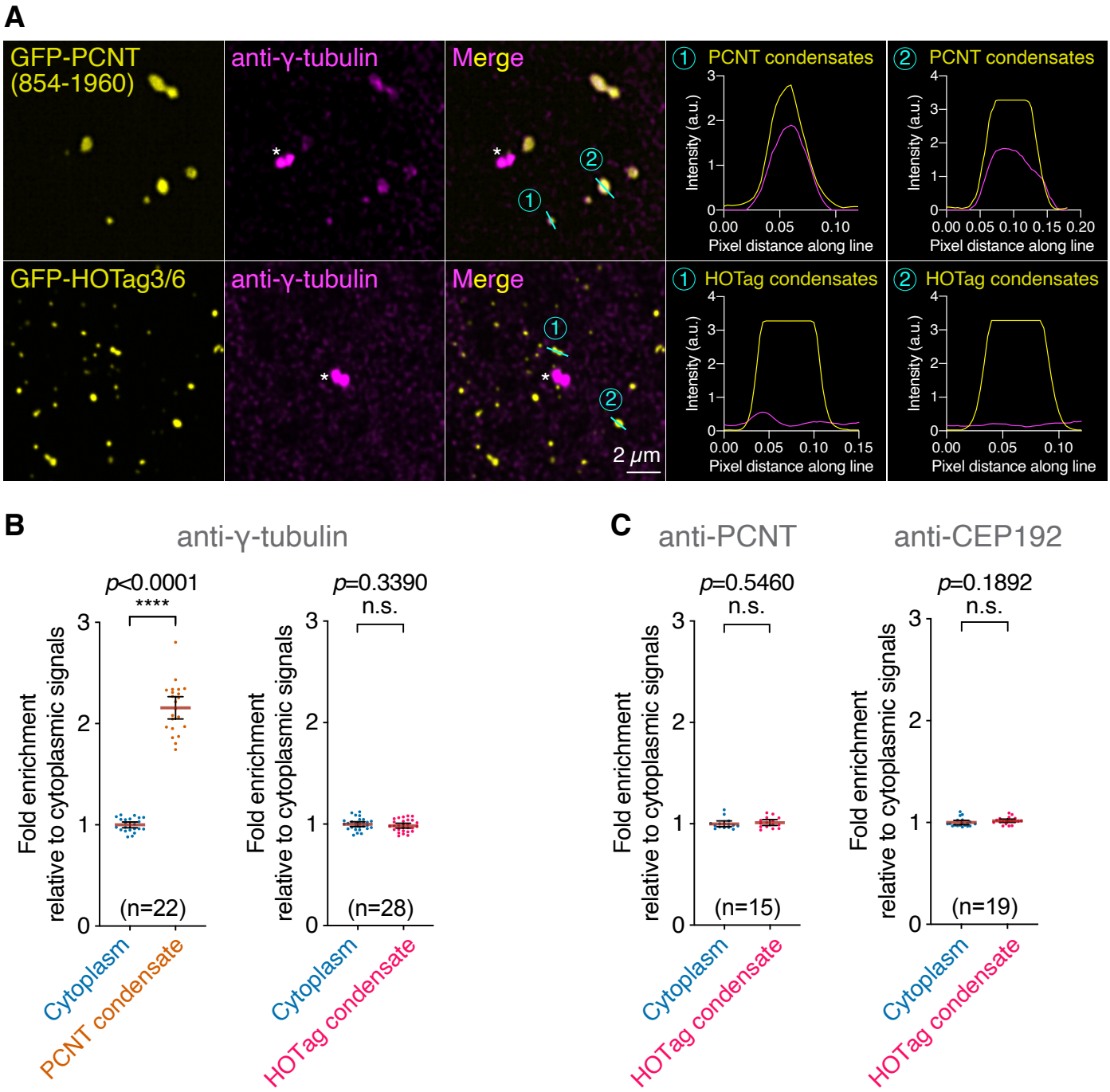

Figure 4- figure supplement 1. Endogenous PCM components are not enriched in the HOTag condensates. (**A**) Anti-γ-tubulin immunofluorescence of GFP-PCNT (854-1960) and GFP-HOTag3/6 condensates. Right: The line plots of the selected regions (cyan lines). Asterisks denote the centrosomes. (**B** and **C**) Fold enrichment of fluorescence signals in the PCNT or HOTag condensates relative to those in the cytoplasm was quantified. Data are mean ± 95% CI. p-values were determined by two-tailed Student's t-test. n.s., not significant. n, number of cells analyzed from two, one, and two biological replicates for γ-tubulin, PCNT, and CEP192, respectively.

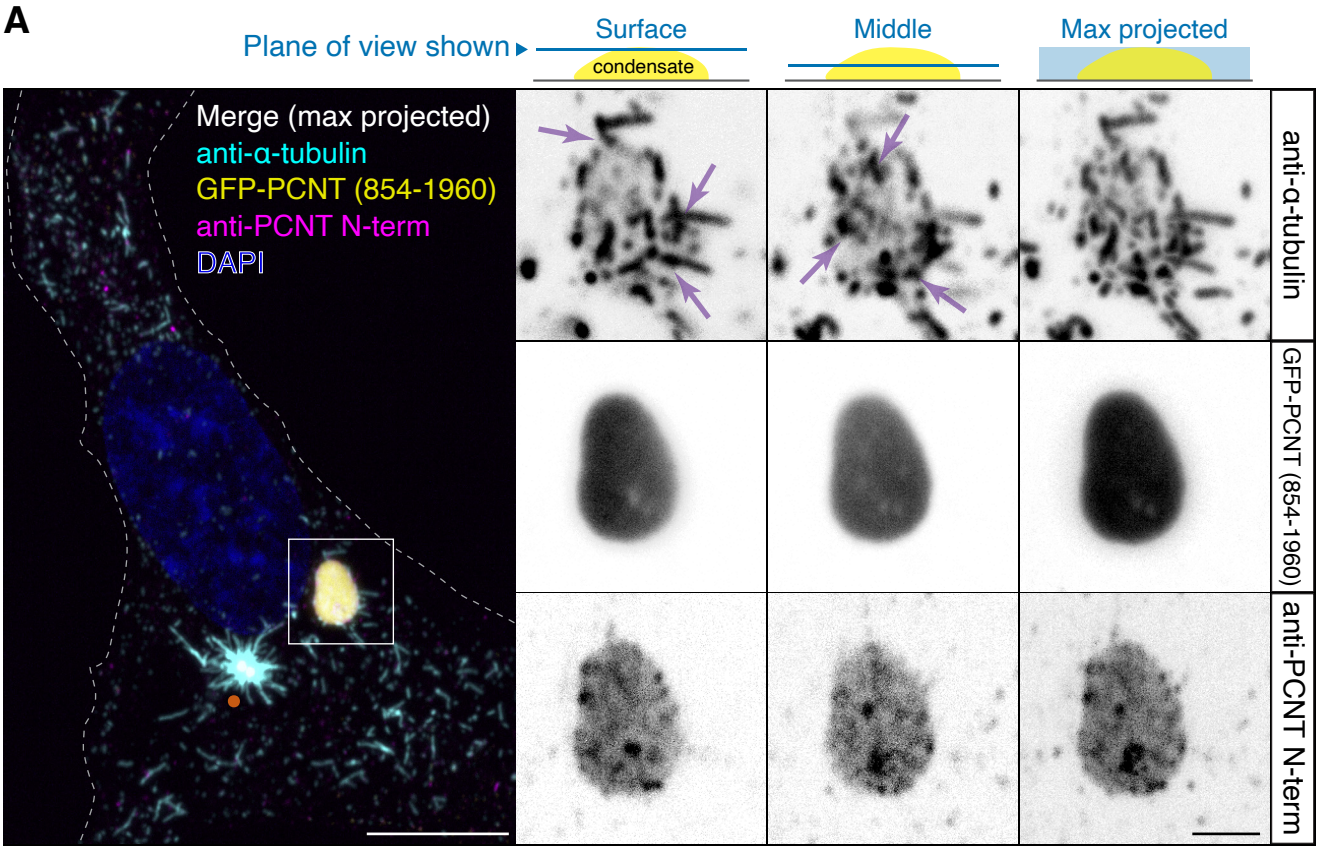

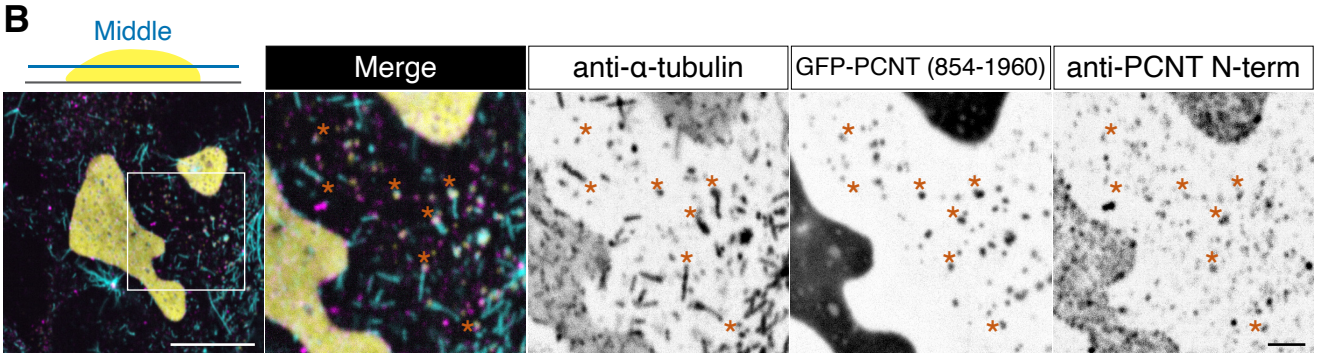

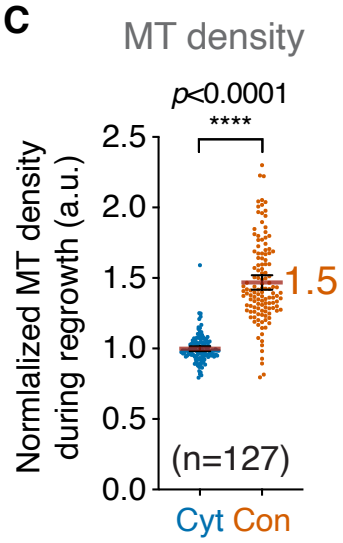

Figure 5. GFP-PCNT (854-1960) condensates nucleate MTs in cells. (**A**) Anti-α-tubulin immunofluorescence of GFP-PCNT (854-1960) condensates during MT renucleation in max-projected and single optical section views. Note that MTs were renucleated within and on the surface of the condensate (arrows). A dot in the merged channels denotes the centrosome, where MT renucleation was robust. (**B**) MT renucleation also occurred in small PCNT condensates (asterisks), which also recruited endogenous PCNT. (**C**) Quantification of MT density in GFP-PCNT (854-1960) condensates (Con) and in the surrounding cytoplasm (Cyt) during MT renucleation. Data are mean ± 95% CI. Fold enrichment mean value is noted. n, number of condensates analyzed from three biological replicates. The p-value was determined by two-tailed Student's t-test. a.u., arbitrary unit. Scale bars, 10 μm and 2 μm (inset).

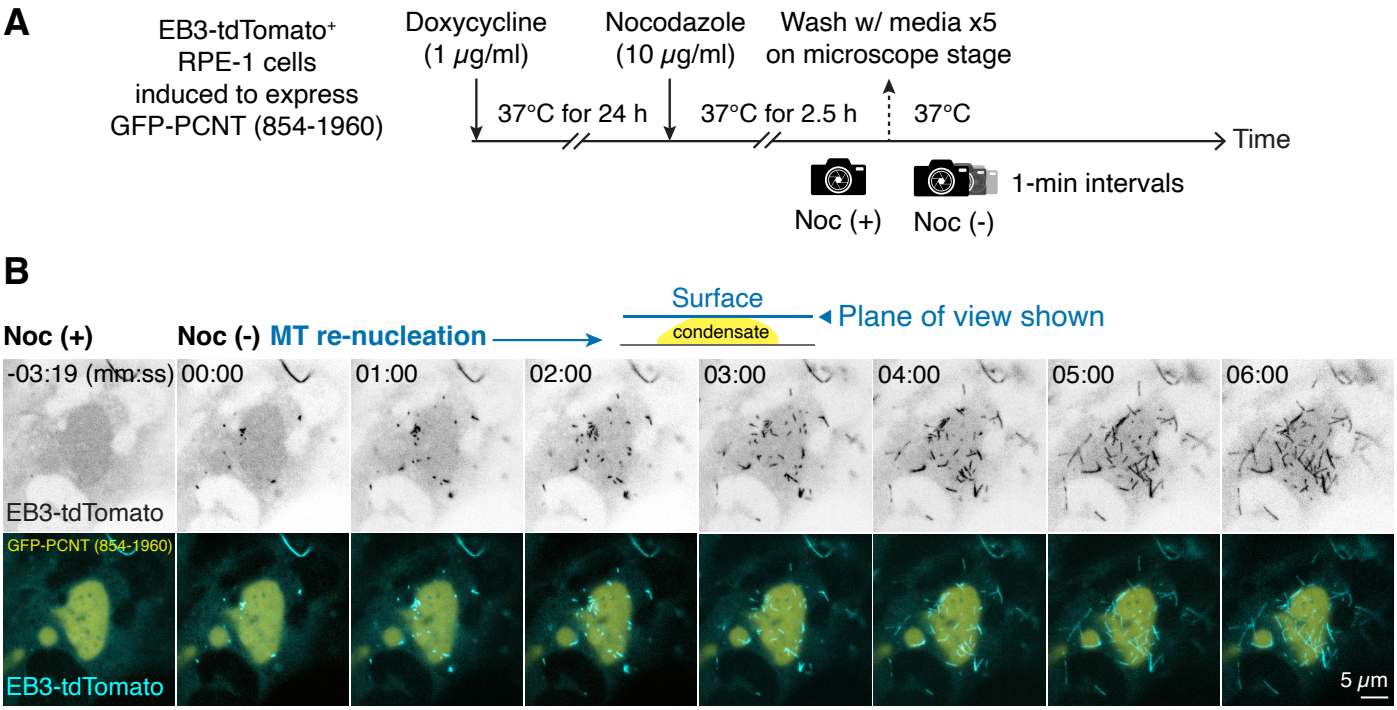

Figure 5- figure supplement 1. GFP-PCNT (854-1960) condensates nucleate MTs in live cells. (**A**) Schematic of the MT renucleation assay in live cells. GFP-PCNT (854-1960) condensates in EB3-tdTomato-positive RPE-1 cells were formed after Dox induction. MTs were then depolymerized by nocodazole (Noc). A pre-wash image was taken [Noc (+)], followed by time-lapse imaging at 1-min intervals after nocodazole was washed out on the microscope stage to follow MT renucleation [Noc (-)]. (**B**) Single optical sections of time-lapse micrographs of EB3-tdTomato-labeled microtubule plus ends on the surface of a GFP-PCNT (854-1960) condensate during MT renucleation. Time 0 was the time immediately after nocodazole was washed out. The experiment was repeated three times with similar results.

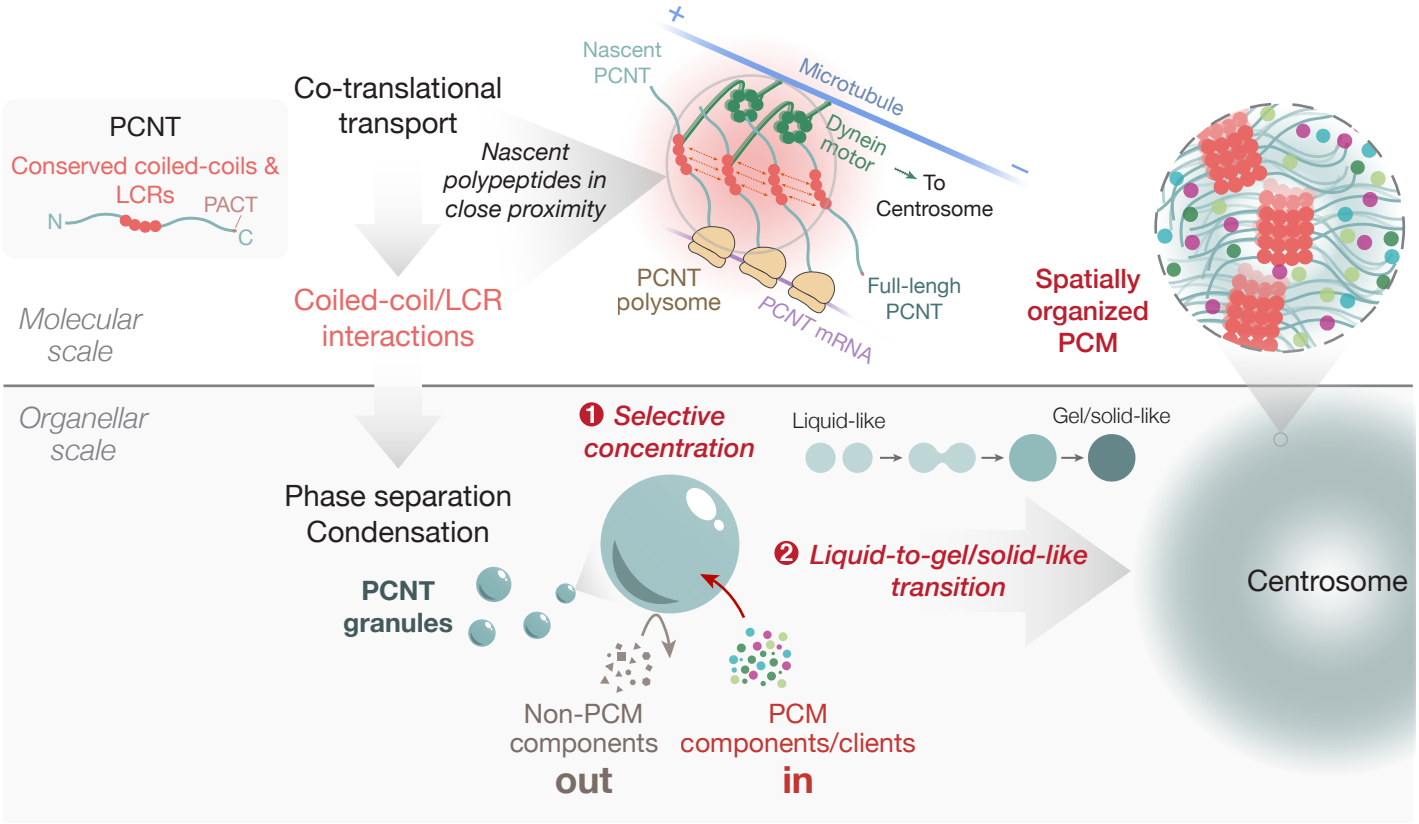

Figure 6. Model for PCNT phase separation in centrosome assembly. PCNT is a linear multivalent protein that phase separates through its conserved coiled-coils and LCRs during its co-translational targeting to the centrosome when the nascent PCNT polypeptides are in close proximity in the polysome. The resulting PCNT granules/condensates promote PCM assembly by (1) selectively concentrating PCM components and clients; this will facilitate and limit the biochemical reactions that eventually take place at the centrosome (e.g., MT nucleation, kinase activities) and (2) enabling a liquid-to-gel/solid-like transitioning process during centrosome assembly; this process provides the PCM components a thermodynamically favored pathway to assemble into a micron-sized, membraneless, and yet spatially organized PCM.